Arab J Geosci (2015) 8:5579–5599
DOI 10.1007/s12517-014-1652-z

ORIGINAL PAPER

The petrogenesis of late Neoproterozoic gabbro/diorite intrusion at Sheikh El-Arab area, central Sinai, Egypt

Michael Dawood Samuel · Doris Sadek Ghabrial · Hilmy Essa Moussa · Mohamed Wahbi Ali-Bik

Received: 23 April 2014 / Accepted: 22 September 2014 / Published online: 7 October 2014

Abstract The late Neoproterozoic gabbro/diorite intrusion (~11.7 km^2) at Sheikh El-Arab area represents the only mafic exposure in the basement rocks of Katharina province of central Sinai largely occupied by granitoids and their volcanic equivalents. The field relations indicate that the intrusion is younger than the lower unit (630–615 Ma) of the volcanics and clastics of the Rutig Formation, and older than the surrounding granodiorites of Sheikh El-Arab and Rahaba (~610 Ma) plutons. It is not affected by regional metamorphism or ductile deformation, but recorded petrographic uralitization/amphibolitization signature. It is composed chiefly of pyroxene-hornblende gabbro, diorite, and quartz diorite. The chemical composition of the mafic minerals indicated that the suite was derived from calc-alkaline magma. Geochemically, the studied rocks are characterized by enrichment of LILE relative to HFSE and LREE relative to HREE. The gabbros are notably low in total REE (38–56 ppm) with $(La/Yb)_n$=2.7–4.8, while the dioritic rocks are high in ΣREE (142–161 ppm) with high $(La/Yb)_n$ values (12.5–15.8); both are characterized by the absence of Eu anomaly, their Eu/Eu* ratios are close to unity (0.93–1.11). The studied intrusion evolved from mafic mantle magma into different types by assimilation fractional crystallization process (AFC) and/or gradual decrease in oxygen fugacity. The initial magma corresponds, most probably, to pyroxene-hornblende gabbro and the crystallization of hornblende was ascribed by slight H_2O increase in magma after crystallization of near-liquidus clinopyroxene with high Ca content ($Wo_{42–52}$) and Ca-rich plagioclase ($An_{80–83}$). The intrusion is related to the later calc-alkaline substage of post-collisional tectonic setting.

M. D. Samuel · D. Sadek Ghabrial (✉) · H. E. Moussa · M. W. Ali-Bik
Geological Sciences Department, National Research Centre, 12662, Dokki Cairo, Egypt
e-mail: dghabrial@yahoo.com

Keywords Neoproterozoic · Sinai · Arabian-Nubian shield · Gabbro/diorite intrusion · Post-collisional setting

Introduction

The basement rocks of Sinai are located in the northernmost outcrops of the Arabian-Nubian Shield (ANS) (Fig. 1). The Shield is a prominent example of juvenile crustal province of Neoproterozoic age (1000–540 Ma) (e.g. Bentor 1985; Stern 1994; Johnson and Woldehaimanot 2003). It is the northern part of the East African Orogen, which is viewed as a collage of island arc complexes accreted during the closure of the Mozambique Ocean between East and West Gondwana (Kröner 1985; Stern 1994; Meert 2003; Jarrar et al. 2003; Stoeser and Frost 2006).

In Sinai, the ANS juvenile crust comprises the island arc complexes (IAC) of pre-collisional stage (~820–740 Ma) and formed of metamorphosed volcano-sedimentary rocks, para- and orthogenesis, associated with migmatites and amphibolites. This is followed by the collisional stage (~670–630 Ma) characterized by the presence of variably deformed calc-alkaline granodiorites, diorites, and gabbros. The Dokhan Volcanics, the mollase sediments, together with mostly undeformed calc-alkaline granitoids, quartz diorites and minor gabbros (~630–590 Ma), and alkaline/peralkaline A-type granites and their equivalent volcanics (~610–580 Ma), are formed during late- to post-collisional stage of the ANS crust evolution (e.g. Stern and Hedge 1985; Stern 1994; Beyth et al. 1994; Abdel-Rahman 1995; Jarrar et al. 2003; Moussa et al. 2008; Be'eri-Shlevin et al. 2009a; Eyal et al. 2010; Farahat et al. 2011). Recently, however, Eyal et al. (2014) recorded shift of ages of similar stages in the northeastern and southern areas of Sinai.

The Neoproterozoic gabbroic rocks constitute one of the distinctive rock units in the Precambrian basement of Egypt.

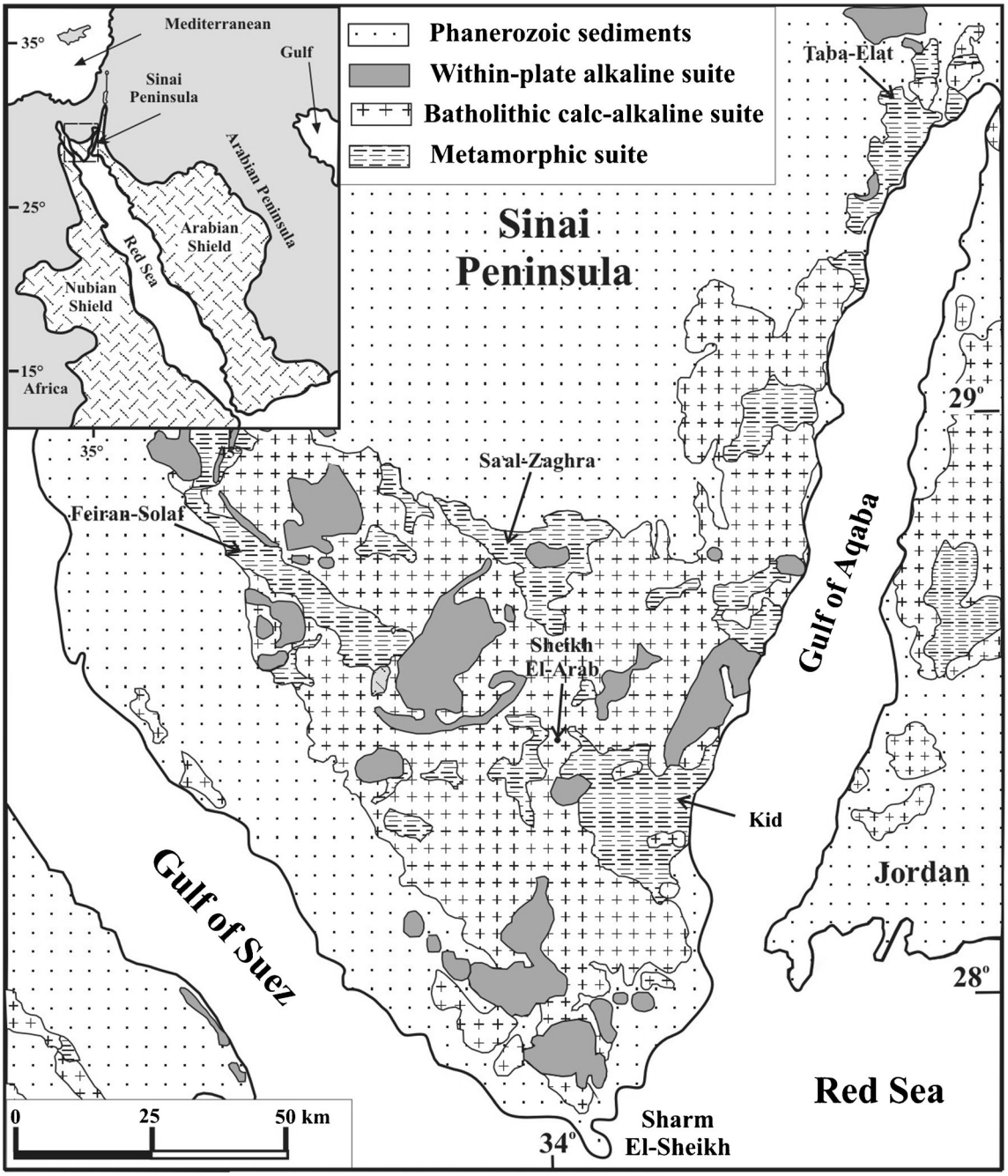

Fig. 1 Simplified geological map of late Neoproterozoic rocks in south Sinai showing the location of the study area (modified after Eyal et al. 1980). *Inset* shows the location of Sinai in the northernmost ANS, along with Neoproterozoic exposures of eastern Africa and western Arabia

Previous studies on these rocks created controversy on their age, origin, and tectonic environment. This controversy exists as a result of the differences in their classification. Basta and Takla (1974), Takla et al. (1981, 2001), Takla (2002) classified these gabbros into older and younger gabbroic suites. The older suite (Older Gabbros) is ophiolitic metagabbros, while the younger suite (Younger Gabbros) is unmetamorphosed, alkali and calc-alkali mafic-ultramafic intrusions of post-tectonic intraplate setting. Bentor (1985) related the gabbroic rocks of the Arabo-Nubian Massif to four phases: the oceanic, island arc, calc-alkaline batholithic, and final alkaline phase. El-Gaby et al. (1988, 1990) and El-Gaby (2007) differentiated these gabbros into (1) ophiolitic metagabbros with tholeiitic affinity, (2) intrusive subduction-related calc-alkaline regionally metamorphosed gabbros (=metagabbro/diorite complexes) which intruded the island arc metavolcanics and metasediments, and (3) tholeiitic olivine gabbro and related rocks intruded at the late cordillera stage. All the above-mentioned classifications negate the presence of ophiolitic mafic-ultramafic assemblages in Sinai. However, several

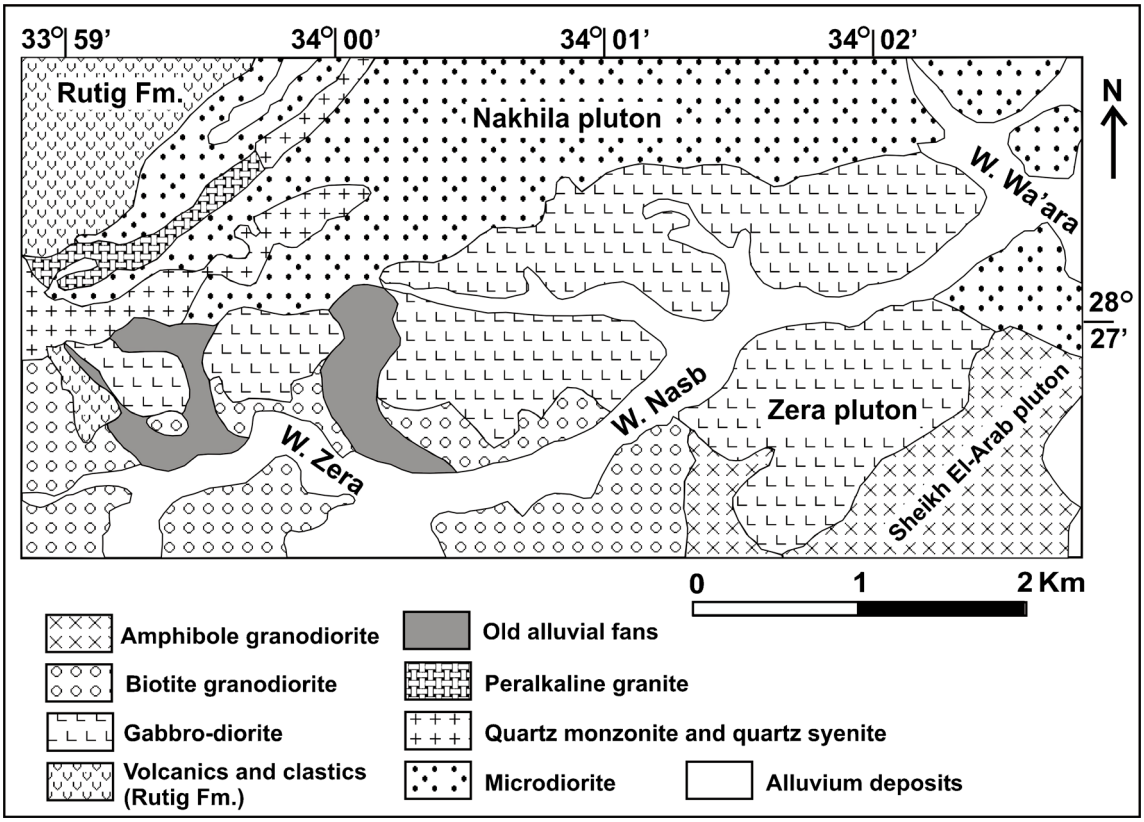

Fig. 2 Geologic map of the gabbro/diorite intrusion at Sheikh El-Arab area, central Sinai (modified after Eyal et al. 2013)

authors interpreted some mafic-ultramafic complexes in south Sinai as fragments of an ophiolitic sequence. The criteria given for their interpretation cannot be substantiated.

Soliman (1996) described Gebel Sheikh El-Arab itself as diorite-granodiorite complex, younger than the gabbro/diorite complex exposed to the north and separated from it by Wadi

Table 1 Modal composition of gabbro/diorite intrusion of Sheikh El-Arab area

Rock type	Sample	Qz	Pl	K-feld	Amp	Cpx	Bt	Chl	Opaques
Py-Hb gabbro	11	–	58.42	–	17.31	13.01	6.80	1.12	3.35
	12	–	56.58	–	25.10	8.33	6.33	0.77	2.83
	13	–	57.51	–	20.83	12.25	6.13	0.83	3.19
	14	–	54.34	–	31.06	6.45	4.83	1.81	3.32
	15	–	59.59	–	25.55	4.31	7.12	0.62	2.81
	16	–	50.49	–	37.17	6.08	3.65	0.61	2.92
Diorite	17A	5.05	68.73	2.01	11.92	2.22	7.48	1.03	2.63
	17B	3.64	70.81	0.99	12.97	2.32	5.56	0.66	3.04
Qz-diorite	1	7.44	65.83	2.58	12.88	1.14	4.87	1.55	3.72
	2	8.72	63.90	3.84	9.49	1.92	6.04	2.88	3.21
	3	9.48	64.96	1.42	13.75	0.95	4.98	0.95	3.51
	4A	8.62	66.64	1.63	11.09	1.86	6.05	0.70	3.40
	4B	9.32	67.87	1.80	8.51	1.35	6.33	0.90	3.89
	4C	8.92	70.02	1.42	7.19	1.83	5.60	1.22	3.82
	4D	8.99	68.65	1.88	10.03	1.25	5.64	0.42	3.14
	4E	8.61	69.34	1.91	8.32	3.11	4.54	0.48	3.68
	6	7.70	68.36	2.25	9.44	2.89	5.20	1.28	2.89
	7	10.19	69.94	1.62	7.04	1.62	6.02	1.11	2.45

Table 2 Representative microprobe analyses of feldspars of the studied intrusion

	Plagioclases										K-feldspars			
	Py-Hb gabbro				Diorite				Qz-diorite					
SiO_2	47.47	46.41	48.76	46.05	57.94	55.73	53.03	55.91	61.10	60.77	59.77	62.71	63.61	62.71
TiO_2	0.02	0.00	0.00	0.00	0.03	0.16	0.02	0.02	0.01	0.02	0.05	0.08	0.01	0.05
Al_2O_3	35.21	35.41	26.11	36.11	27.88	28.77	28.39	27.89	25.63	25.05	26.60	20.01	19.90	20.17
FeO	0.13	0.22	0.17	0.14	0.21	0.26	0.17	0.05	0.05	0.08	0.32	0.03	0.05	0.09
MnO	0.04	0.03	0.02	0.00	0.00	0.00	0.03	0.06	0.00	0.02	0.03	0.02	0.00	0.00
MgO	0.01	0.06	0.07	0.04	0.01	0.00	0.08	0.00	0.02	0.00	0.19	0.01	0.01	0.01
CaO	16.96	16.93	21.07	17.06	7.66	9.16	8.89	7.61	5.21	4.62	2.16	0.03	0.00	0.03
Na_2O	2.22	2.18	2.77	1.95	7.14	6.29	5.53	7.10	8.60	8.65	7.98	0.75	0.64	1.12
K_2O	0.04	0.14	0.17	0.07	0.08	0.27	0.60	0.12	0.18	0.32	2.80	14.84	15.36	14.47
P_2O_5	0.04	0.00	0.06	0.00	0.00	0.00	0.02	0.01	0.06	0.01	0.04	0.06	0000	0.00
Total	102.14	101.38	99.20	101.42	100.95	100.64	96.76	98.77	100.86	99.54	99.94	98.53	99.58	98.65
Number of cations on the basis of 8 oxygens														
Si	2.136	2.109	2.302	2.089	2.567	2.492	2.468	2.536	2.689	2.708	2.669	2.928	2.943	2.924
Ti	0.001	0.000	0.000	0.000	0.001	0.005	0.001	0.001	0.000	0.001	0.002	0.003	0.000	0.002
Al	1.865	1.895	1.452	1.929	1.454	1.515	1.556	1.490	1.328	1.315	1.399	1.100	1.084	1.107
Fe^{2+}	0.005	0.008	0.007	0.005	0.008	0.010	0.007	0.002	0.002	0.003	0.012	0.001	0.002	0.004
Mn	0.002	0.001	0.001	0.000	0.000	0.000	0.001	0.002	0.000	0.001	0.001	0.001	0.000	0.000
Mg	0.001	0.004	0.005	0.003	0.001	0.000	0.006	0.000	0.001	0.000	0.013	0.001	0.001	0.001
Ca	0.818	0.824	1.066	0.829	0.364	0.439	0.443	0.370	0.246	0.221	0.103	0.002	0.000	0.001
Na	0.194	0.192	0.254	0.172	0.613	0.545	0.499	0.624	0.734	0.747	0.691	0.068	0.057	0.101
K	0.002	0.008	0.010	0.004	0.005	0.015	0.036	0.007	0.010	0.018	0.160	0.884	0.907	0.861
Total	5.024	5.041	5.097	5.031	5.013	5.021	5.017	5.032	5.010	5.014	5.050	4.988	4.994	5.001
Ab	19.1	18.8	19.1	17.1	62.4	54.6	51.0	62.3	74.1	75.8	72.4	7.1	5.9	10.5
An	80.7	80.5	80.2	82.5	37.1	43.9	45.3	37.0	24.8	22.4	10.8	0.2	0.0	0.1
Or	0.2	0.8	0.8	0.4	0.5	1.5	3.7	0.7	1.0	1.8	16.8	92.7	94.1	89.4
Name	Byt	Byt	Byt	Byt	And	And	And	And	Olig	Olig	Anth	Orth	Orth	Orth

Byt bytownite, *And* andesine, *Olig* oligoclase, *Anth* anorthoclase, *Orth* orthoclase

Table 3 Representative microprobe analyses of pyroxenes of the studied intrusion

Py-Hb gabbro																Diorite		
SiO_2	50.16	51.43	51.99	51.32	52.06	52.70	52.55	51.47	48.98	49.82	51.92	51.70	51.54	51.18	51.62	51.08	48.86	49.27
TiO_2	0.54	0.19	0.26	0.21	0.18	0.12	0.08	0.62	0.48	0.48	0.35	0.18	0.17	0.26	0.11	0.51	0.20	0.73
Al_2O_3	4.73	2.76	2.20	2.01	1.95	1.19	0.65	0.58	4.70	4.78	2.47	1.58	0.82	2.74	1.56	1.84	1.32	3.96
FeO	9.47	6.69	6.85	7.15	7.08	7.04	6.91	6.96	7.90	8.53	7.26	7.53	7.75	8.11	7.38	8.43	7.84	9.36
MnO	0.28	0.21	0.12	0.18	0.22	0.21	0.26	0.25	0.16	0.12	0.21	0.27	0.25	0.19	0.30	0.30	0.26	0.26
MgO	14.37	14.24	15.10	14.82	14.79	14.76	14.30	13.52	14.31	14.40	14.26	13.95	13.93	14.29	14.10	13.85	13.65	13.66
CaO	19.77	24.00	23.26	23.41	23.68	24.10	24.96	26.15	21.54	23.61	23.81	23.87	23.47	21.76	24.31	22.54	23.69	19.83
Na_2O	0.60	0.28	0.31	0.23	0.25	0.17	0.14	0.12	0.62	0.60	0.24	0.18	0.26	0.41	0.18	0.36	0.30	0.55
K_2O	0.24	0.02	0.26	0.02	0.01	0.02	0.01	0.01	0.12	0.14	0.00	0.01	0.01	0.11	0.02	0.02	0.06	0.61
P_2O_5	0.00	0.03	0.00	0.01	0.00	0.00	0.02	0.00	0.16	0.03	0.11	0.00	0.08	0.04	0.10	0.03	0.11	0.01
Total	100.16	99.85	100.35	99.36	100.22	100.31	99.88	99.68	98.97	99.51	100.63	99.27	99.28	99.09	99.68	98.96	96.29	98.24
Number of cations on the basis of 6 oxygens																		
Si	1.851	1.903	1.908	1.907	1.919	1.944	1.951	1.923	1.824	1.846	1.913	1.934	1.928	1.912	1.922	1.919	1.884	1.859
Al	0.206	0.120	0.095	0.088	0.085	0.052	0.028	0.026	0.207	0.209	0.107	0.069	0.080	0.120	0.068	0.082	0.060	0.177
Ti	0.015	0.005	0.007	0.006	0.005	0.003	0.002	0.017	0.013	0.013	0.010	0.005	0.005	0.007	0.003	0.014	0.006	0.021
Fe^{3+}	0.115	0.084	0.108	0.103	0.086	0.066	0.075	0.103	0.168	0.121	0.065	0.067	0.074	0.076	0.094	0.078	0.185	0.133
Fe^{2+}	0.177	0.123	0.102	0.120	0.133	0.151	0.140	0.114	0.078	0.143	0.158	0.169	0.169	0.177	0.136	0.187	0.067	0.163
Mn	0.009	0.007	0.004	0.006	0.007	0.007	0.008	0.008	0.005	0.004	0.007	0.009	0.008	0.006	0.009	0.010	0.008	0.008
Mg	0.791	0.785	0.826	0.821	0.813	0.812	0.792	0.753	0.788	0.796	0.783	0.778	0.777	0.796	0.783	0.776	0.785	0.769
Ca	0.782	0.951	0.915	0.932	0.935	0.952	0.993	1.047	0.860	0.818	0.940	0.956	0.941	0.871	0.970	0.907	0.979	0.802
Na	0.043	0.020	0.022	0.017	0.018	0.012	0.010	0.009	0.045	0.043	0.017	0.013	0.019	0.030	0.013	0.026	0.022	0.040
K	0.011	0.001	0.012	0.001	0.000	0.001	0.000	0.000	0.006	0.007	0.000	0.000	0.000	0.005	0.001	0.001	0.003	0.029
Total	4.000	3.999	3.999	4.001	4.001	4.000	3.999	4.000	3.994	4.000	4.000	4.000	4.001	4.000	3.999	4.000	3.999	4.001
Wo	41.73	48.78	46.79	47.05	47.40	47.91	49.47	51.69	45.12	43.48	48.12	48.35	47.80	45.22	48.69	46.35	48.34	42.79
En	42.20	40.27	42.26	41.45	41.19	40.83	39.43	37.18	41.70	42.27	40.10	39.31	39.48	41.32	39.30	39.63	38.75	41.01
Fs	16.07	10.95	10.95	11.50	11.41	11.26	11.10	11.13	13.18	14.25	11.79	12.34	12.72	13.47	12.01	14.02	12.91	16.21
Name	Aug	Dio	Dio	Dio	Dio	Dio	Dio	Dio	Dio	Aug	Dio	Dio	Dio	Dio	Dio	Dio	Dio	Aug

Aug augite, *Dio* diopside

Table 4 Representative microprobe analyses of amphiboles of the studied intrusion

	Py-Hb gabbro																	
	Primary amphiboles							Secondary amphiboles										
SiO_2	42.89	44.99	43.80	44.53	43.75	44.45	44.31	48.39	49.33	50.28	49.71	53.37	54.16	53.94	53.51	54.92	52.10	52.66
TiO_2	1.03	0.96	0.94	0.94	0.98	1.10	1.03	0.56	0.04	0.08	0.00	0.06	0.06	0.15	0.16	0.11	0.31	0.27
Al_2O_3	12.22	10.52	11.12	10.46	11.79	11.14	11.23	6.05	6.66	5.91	6.74	2.88	1.66	2.33	2.37	1.24	3.52	3.29
FeO	14.93	13.43	13.94	14.07	14.84	12.81	14.64	8.68	12.89	11.70	12.38	10.69	10.12	10.41	10.02	9.83	10.92	11.32
MnO	0.31	0.26	0.26	0.32	0.26	0.21	0.28	0.10	0.29	0.23	0.26	0.29	0.26	0.25	0.21	0.23	0.24	0.24
MgO	11.58	13.37	12.58	12.75	11.98	12.87	12.16	14.80	15.28	15.60	15.20	17.28	18.40	17.59	17.89	17.84	16.47	16.46
CaO	11.92	12.07	12.21	12.43	12.12	12.79	12.27	17.34	12.39	12.50	12.24	12.46	12.40	12.70	12.70	12.99	12.86	12.62
Na_2O	1.47	1.35	1.30	1.24	1.42	1.30	1.31	0.74	0.78	0.67	0.75	0.32	0.17	0.22	0.28	0.15	0.44	0.35
K_2O	0.64	0.64	0.76	0.57	0.67	0.64	0.63	0.11	0.17	0.20	0.24	0.10	0.05	0.08	0.08	0.04	0.10	0.14
P_2O_5	0.00	0.04	0.00	0.00	0.07	0.00	0.00	0.10	0.04	0.03	0.00	0.00	0.00	0.00	0.15	0.06	0.00	0.07
Total	96.99	97.63	96.91	97.31	97.88	97.31	97.86	96.87	97.87	97.20	97.52	97.45	97.28	97.67	97.37	97.41	96.96	97.42
Number of cations on the basis of 23 oxygens																		
Si	6.380	6.589	6.485	6.554	6.443	6.525	6.512	6.985	7.096	7.257	7.170	7.617	7.696	7.666	7.626	7.817	7.504	7.561
Al^{IV}	1.620	1.411	1.515	1.446	1.557	1.475	1.488	1.015	0.904	0.743	0.830	0.383	0.278	0.334	0.374	0.183	0.496	0.439
Al^{VI}	0.521	0.404	0.423	0.367	0.488	0.451	0.456	0.013	0.224	0.261	0.315	0.101	0.000	0.056	0.023	0.024	0.101	0.118
Ti	0.115	0.106	0.105	0.104	0.109	0.121	0.114	0.061	0.004	0.009	0.000	0.006	0.006	0.016	0.017	0.012	0.034	0.029
Fe^{3+}	0.323	0.292	0.366	0.410	0.320	0.290	0.313	0.653	0.423	0.240	0.261	0.163	0.261	0.171	0.225	0.087	0.187	0.140
Fe^{2+}	1.534	1.353	1.361	1.321	1.508	1.282	1.486	0.394	1.127	1.172	1.233	1.114	0.942	1.066	0.970	1.083	1.129	1.219
Mn	0.039	0.032	0.033	0.040	0.032	0.026	0.035	0.012	0.035	0.028	0.032	0.035	0.031	0.030	0.025	0.028	0.029	0.029
Mg	2.568	2.919	2.777	2.797	2.630	2.817	2.664	3.185	3.277	3.357	3.268	3.676	3.898	3.727	3.801	3.785	3.536	3.523
Ca	1.900	1.894	1.937	1.960	1.913	2.012	1.932	2.682	1.909	1.953	1.892	1.905	1.888	1.934	1.939	1.981	1.985	1.941
Na	0.424	0.383	0.373	0.354	0.406	0.370	0.373	0.207	0.218	0.188	0.210	0.089	0.047	0.061	0.077	0.041	0.123	0.097
K	0.121	0.120	0.144	0.107	0.126	0.120	0.118	0.020	0.031	0.037	0.044	0.018	0.009	0.015	0.015	0.007	0.018	0.026
Name	Tsch	Mg-Hb	Tsch	Mg-Hb	Tsch	Mg-Hb	Tsch	Mg-Hb	Mg-Hb	Mg-Hb	Mg-Hb	Act	Act	Act	Act	Act	Mg-Hb	Act
	Py-Hb gabbro								Diorite									
	Secondary amphiboles								Prim. amph.	Secondary amphiboles								
SiO_2	50.56	51.07	51.16	50.86	46.98	46.88	47.57	50.10	47.12	54.18	53.02	52.43	49.27	48.05	50.29	53.09	50.15	51.76
TiO_2	0.43	0.21	0.20	0.29	0.51	0.6	0.53	0.81	4.14	0.11	0.11	0.30	0.47	0.71	0.67	0.10	0.23	0.16
Al_2O_3	5.14	4.59	4.25	5.26	8.28	8.66	8.12	4.82	2.54	1.34	1.54	2.27	3.74	5.21	4.52	0.96	3.96	2.85
FeO	12.79	12.37	12.03	12.80	12.36	13.69	13.40	14.26	12.81	10.95	10.70	11.95	12.65	14.17	13.30	10.83	12.92	12.01
MnO	0.27	0.26	0.28	0.25	0.22	0.26	0.33	0.27	0.52	0.41	0.30	0.30	0.30	0.39	0.34	0.34	0.24	0.29
MgO	14.55	15.31	15.63	14.98	13.45	13.51	13.18	12.41	13.68	16.82	16.67	15.88	14.52	13.77	14.87	16.69	14.68	15.32
CaO	12.65	12.56	12.47	12.74	12.59	12.59	12.78	12.68	16.92	12.97	12.93	12.58	12.88	12.55	12.45	12.46	13.13	13.81
Na_2O	0.57	0.54	0.43	0.59	0.92	1.05	0.89	1.12	0.44	0.25	0.25	0.33	0.39	0.64	0.69	0.20	0.40	0.30
K_2O	0.26	0.18	0.12	0.19	0.39	0.33	0.24	0.47	0.12	0.07	0.07	0.15	0.21	0.41	0.36	0.09	0.22	0.11

Table 4 (continued)

P_2O_5	0.00	0.00	0.09	0.00	0.04	0.00	0.00	0.06	0.04	0.00	0.04	0.00	0.03	0.07	0.05	0.00	0.04	0.00
Total	97.22	97.09	96.66	97.96	95.74	97.57	97.04	97.00	98.33	97.10	95.63	96.19	94.46	95.96	97.54	94.76	95.97	96.61
Number of cations on the basis of 23 oxygens																		
Si	7.365	7.403	7.431	7.324	6.914	6.839	6.971	7.074	6.869	7.791	7.735	7.656	7.368	7.145	7.321	7.817	7.379	7.526
Al^{IV}	0.635	0.597	0.569	0.676	1.086	1.161	1.029	0.890	0.436	0.209	0.265	0.344	0.632	0.855	0.679	0.166	0.621	0.474
Al^{VI}	0.245	0.186	0.158	0.216	0.348	0.326	0.372	0.000	0.000	0.018	0.000	0.046	0.027	0.057	0.096	0.000	0.065	0.014
Ti	0.047	0.023	0.022	0.031	0.056	0.066	0.058	0.096	0.454	0.012	0.012	0.033	0.053	0.097	0.073	0.011	0.025	0.017
Fe^{3+}	0.105	0.180	0.225	0.198	0.289	0.345	0.242	0.335	0.772	0.085	0.159	0.111	0.347	0.376	0.174	0.103	0.350	0.320
Fe^{2+}	1.451	1.319	1.237	1.343	1.343	1.325	1.400	1.536	0.790	1.231	1.147	1.348	1.235	1.386	1.445	1.231	1.240	1.141
Mn	0.033	0.012	0.034	0.030	0.027	0.012	0.041	0.036	0.064	0.050	0.037	0.037	0.038	0.050	0.042	0.042	0.030	0.036
Mg	3.156	3.308	3.384	3.216	2.951	2.938	2.879	2.902	2.973	3.606	3.625	3.457	3.237	3.052	3.227	3.664	3.220	3.321
Ca	1.972	1.951	1.941	1.966	1.985	1.968	2.007	2.131	2.643	1.998	2.021	1.968	2.064	1.999	1.942	1.966	2.000	2.151
Na	0.161	0.152	0.121	0.165	0.263	0.297	0.253	0.341	0.124	0.070	0.071	0.093	0.113	0.185	0.195	0.057	0.114	0.085
K	0.048	0.033	0.022	0.035	0.073	0.061	0.045	0.094	0.022	0.013	0.013	0.028	0.040	0.078	0.067	0.017	0.041	0.020
Name	Mg-Hb	Mg-Hb	Mg-Hb	Mg-Hb	Mg-Hb	Mg-Hb	Mg-Hb	Mg-Hb	Mg-Hb	Act	Act	Act	Mg-Hb	Mg-Hb	Mg-Hb	Act	Mg-Hb	Act

Tsch tschermakite, *Mg-Hb* magnesio-hornblende, *Act* actinolite

Nasb. At the intersection between Wadi Nasb and Wadi Rahaba, the gabbro/diorite rocks intruded mafic-ultramafic rocks; the latter, interpreted to represent fault-bounded fragments of oceanic crust or fault slivers of rocks originally, were intrusive-extrusive complexes. Soliman (op. cit.) regarded all the above-mentioned rock types older than the Rutig volcanics and volcanoclastics. In addition, questionable geochemical data were given for only three samples of mafic-ultramafic rocks. They have 50.10–56.65 wt.% SiO_2, 3.56–4.25 wt.% Na_2O, 1.45–4.92 wt.% K_2O, 542–880 ppm Ba, 1.5–5.9 ppm Co, and Y is not detected.

Abdel-Karim (2013) described only a small gabbroic mass to the east of Wadi Rahaba formed of uralitized gabbro and hornblendite. It intruded the Older granitoids (calc-alkaline tonalite-granodiorite association) with sharp contacts, and in turn, intruded by Younger granites (calc-alkaline to alkaline granodiorite to alkali-feldspar granites). The uralitized gabbros are composed of cumulus augite (45 %) and hypersthene and plagioclase (40 %) with subordinate hornblende and quartz. The hornblendites are composed of cumulus hornblende (62 %) and plagioclase (30 %) with minor pyroxene, biotite, and quartz. Their parental magma is tholeiitic in nature and was mostly generated and emplaced in continental crust and tends to be formed by a transitional compression-extension regime dominated from the final arc stage to active continental margin. The above-mentioned petrographic nomenclature contradicts the IUGS classification. The petrogenetic aspects of the Rahaba intrusion as given by Abdel-Karim (2013) are difficult to accept as the transitional compression-extension regime in Sinai extending from ~740 to ~610 Ma.

The present study deals with the geological, petrographical, mineralogical, and geochemical characteristics of the gabbro/diorite intrusion at Gebel Sheikh El-Arab area (central Sinai) in order to explain its tectonic setting and petrogenesis. In addition, the new data presented here will determine if these gabbro/diorite rocks are related as previously thought to the older metagabbro/diorite complexes or to the younger gabbros. Also, the data, together with the previously published ones concerning gabbroic rocks in south Sinai, may shed light on its evolution.

Geologic setting

The oldest basement rock units in Katharina province include remnants of older metavolcanics and metasediments of unknown age. A younger tectonomagmatic cal-alkaline phase in the province is characterized by vast intrusion of weakly to non-deformed calc-alkaline plutons and volcano-sedimentary succession (Rutig Formation). The calc-alkaline magmatic phase is separated from the overlying alkaline magmatic phase by Hamad Abadu unconformity and Katharina Group. The latter constitutes a stratified sequence of pyroclastics,

Table 5 Representative microprobe analyses of biotites of the studied intrusion

	Py-Hb gabbro		Diorite												
SiO_2	35.84	36.33	36.86	36.57	36.49	36.76	36.27	37.13	36.70	36.37	36.32	35.51	36.51	35.26	35.24
TiO_2	3.71	3.94	2.96	2.68	3.03	2.68	2.67	2.10	1.96	2.24	2.73	1.20	2.13	1.10	1.04
Al_2O_3	14.09	13.70	15.53	15.32	15.12	15.32	15.31	15.72	15.77	15.82	15.05	16.19	15.09	18.26	18.75
FeO	19.52	18.99	18.30	18.25	18.41	18.45	17.91	17.94	17.83	17.78	18.05	17.71	17.70	17.13	17.04
MnO	0.20	0.22	0.14	0.24	0.19	0.14	0.21	0.17	0.18	0.20	0.18	0.20	0.20	0.16	0.17
MgO	12.96	12.44	11.49	12.14	11.57	12.25	12.21	12.24	12.29	11.83	12.36	12.59	12.51	12.77	12.84
CaO	0.04	0.13	0.06	0.11	0.05	0.07	0.03	0.01	0.04	0.00	0.03	0.04	0.04	0.09	0.04
Na_2O	0.12	0.16	0.13	0.11	0.19	0.11	0.16	0.12	0.16	0.13	0.20	0.09	0.14	0.08	0.12
K_2O	8.80	8.45	8.88	8.87	8.91	8.70	8.91	9.13	9.01	9.31	8.84	8.58	8.45	8.87	8.98
P_2O_5	0.01	0.00	0.13	0.01	0.03	0.02	0.01	0.00	0.04	0.00	0.00	0.05	0.02	0.05	0.00
Total	95.29	94.36	94.48	94.30	93.99	94.50	93.69	94.56	93.98	93.68	93.75	92.17	92.79	93.77	94.22
Number of cations on the basis of 22 oxygens															
Si	5.495	5.595	5.630	5.608	5.621	5.618	5.595	5.662	5.631	5.613	5.602	5.554	5.662	5.400	5.370
Al^{IV}	2.505	2.405	2.370	2.392	2.379	2.382	2.405	2.338	2.369	2.387	2.398	2.446	2.338	2.600	2.630
Al^{VI}	0.039	0.080	0.423	0.375	0.364	0.375	0.377	0.485	0.481	0.488	0.336	0.536	0.416	0.693	0.735
Ti	0.428	0.456	0.340	0.309	0.351	0.308	0.310	0.241	0.226	0.260	0.317	0.141	0.248	0.127	0.119
Fe^{2+}	2.503	2.446	2.337	2.341	2.372	2.358	2.311	2.288	2.288	2.295	2.328	2.317	2.295	2.194	2.172
Mn	0.026	0.029	0.018	0.031	0.025	0.018	0.027	0.022	0.023	0.026	0.024	0.026	0.028	0.021	0.022
Mg	2.962	2.856	2.616	2.776	2.657	2.791	2.808	2.782	2.811	2.722	2.842	2.936	2.892	2.916	2.917
Ca	0.007	0.021	0.010	0.018	0.008	0.011	0.005	0.002	0.007	0.000	0.005	0.007	0.007	0.015	0.007
Na	0.036	0.048	0.038	0.033	0.057	0.033	0.048	0.035	0.048	0.039	0.060	0.027	0.042	0.024	0.035
K	1.721	1.660	1.730	1.735	1.751	1.696	1.754	1.776	1.764	1.833	1.740	1.712	1.672	1.733	1.746
Total	15.722	15.596	15.512	15.618	15.585	15.59	15.64	15.631	15.648	15.663	15.652	15.702	15.60	15.723	15.753
Fe/Fe + Mg	0.46	0.46	0.47	0.46	0.47	0.46	0.45	0.45	0.45	0.46	0.45	0.44	0.44	0.43	0.43

ignimbrites together with typical rhyolitic flows of alkaline/peralkaline affinity. The younger alkaline magmatic phase comprises riebeckite granite, monzonite, syenite, syenogranite, and perthite granite.

The Sheikh El-Arab area lies at about 15 km to the southeast of Saint Katharina town. The area is characterized by moderate to high relief terrain and dissected by numerous structurally controlled wadis; namely Wadi Nasb, Wadi Wa'ara, Wadi Zera, and Wadi Rahaba. Gebel Sheikh El-Arab itself is formed of granodiorite pluton surrounded by gabbro/diorite rocks exposed in an area of about 11.7 km^2 and delineated by latitudes 28° 26′ 14″ to 28° 27′ 33″ N and longitudes 33° 59′ 00″ to 34° 02′ 27″ E (Fig. 2). The contact between the studied gabbro/diorite suite and its country rocks are sharp. This suite is generally undeformed and shows no signs of metamorphism. Volcanic and clastic xenoliths of Rutig Formation are included in the gabbro/diorite intrusion.

The investigated gabbro/diorite intrusion crops out as five small masses separated by old alluvial fans and alluvium deposits. Amphibole granodiorite of Sheikh El-Arab pluton and biotite granodiorite of Rahaba pluton (610 Ma; Moreno et al. 2012) intruded the southern parts of the gabbro/diorite masses. The northern parts were intruded by both the Nakhila microdiorite as well as quartz monzonite and quartz syenite of Katharina Outer Ring dyke. The westernmost gabbro/diorite mass intrudes the volcanics and clastics of the lower unit of the Rutig Formation (~630–615 Ma; Be'eri-Shlevin et al. 2011).

Field study showed that the intrusion is heterogeneous comprising gabbros and dioritic rocks; the latter are exposed in small area relative to the gabbros. The contact between the gabbro and dioritic rocks is hardly discerned in the outcrop, only slight color variation can be recognized.

The investigated gabbro/diorite suite is a Neoproterozoic intrusion that was emplaced prior to 610±5 Ma (Moreno et al. 2012), most probably related to the post-collisional calc-alkaline suite, even without direct geochronological data yet. The available U-Pb zircon data (Be'eri-Shlevin et al. 2011; Samuel et al. 2011) show that in Katharina province the emplacement of the lower unit of the Rutig Formation, truncated by the studied gabbro/diorite rocks, lasted from 630 to 615 Ma.

Petrography

Following the IUGS recommendation (1989), the studied intrusion is lithologically classified into gabbro and diorite. The average An content of the plagioclase in the former is

Table 6 Representative microprobe analyses of Fe-Ti oxides of the studied intrusion

	Py-Hb gabbro								Qz-diorite				
	Magnetite							Ilmenite	Ilmenite				
SiO_2	0.02	0.04	0.04	0.04	0.02	0.11	0.04	0.18	0.02	0.00	0.05	0.04	0.02
TiO_2	0.26	0.06	0.03	0.12	0.16	0.10	0.08	48.48	48.73	46.43	48.23	48.05	46.44
Al_2O_3	0.05	0.10	0.11	0.13	0.14	0.11	0.12	0.02	0.01	0.00	0.03	0.03	0.02
FeO	90.17	92.55	92.12	91.57	91.83	91.59	91.89	43.91	46.10	48.52	45.80	46.12	47.74
MnO	0.07	0.00	0.02	0.05	0.00	0.06	0.02	3.68	3.02	2.60	2.85	3.03	2.75
MgO	0.00	0.00	0.05	0.01	0.00	0.05	0.00	0.04	0.18	0.25	0.25	0.13	0.26
CaO	0.01	0.00	0.00	0.00	0.01	0.02	0.01	0.56	0.00	0.02	0.01	0.03	0.03
Na_2O	0.01	0.02	0.02	0.02	0.00	0.03	0.00	0.01	0.09	0.01	0.05	0.03	0.03
K_2O	0.02	0.00	0.02	0.00	0.00	0.00	0.02	0.03	0.00	0.01	0.00	0.00	0.01
P_2O_5	0.00	0.00	0.05	0.00	0.01	0.00	0.00	0.00	0.00	0.00	0.00	0.02	0.00
Total	90.61	92.77	92.46	91.94	92.17	92.07	92.18	96.91	98.15	97.84	97.27	97.48	97.30
Number of cations on the basis of 4 oxygens for magnetite and of 3 oxygens for ilmenite													
Si	0.001	0.002	0.002	0.002	0.001	0.004	0.002	0.005	0.001	0.000	0.001	0.001	0.001
Al	0.002	0.005	0.005	0.006	0.006	0.005	0.006	0.001	0.000	0.000	0.001	0.001	0.001
Ti	0.008	0.002	0.001	0.004	0.005	0.003	0.002	0.945	0.938	0.924	0.936	0.932	0.900
Fe^{3+}	1.980	1.989	1.988	1.984	1.982	1.980	1.987	0.100	0.120	0.152	0.123	0.133	0.199
Fe^{2+}	1.006	1.003	0.999	1.003	1.005	1.001	1.003	0.852	0.867	0.855	0.865	0.861	0.830
Mn	0.002	0.000	0.001	0.002	0.000	0.002	0.001	0.081	0.066	0.058	0.062	0.066	0.060
Mg	0.000	0.000	0.003	0.001	0.000	0.003	0.000	0.002	0.007	0.010	0.010	0.005	0.010
Ca	0.000	0.000	0.000	0.000	0.000	0.001	0.000	0.016	0.000	0.001	0.000	0.001	0.001
Na	0.001	0.002	0.002	0.002	0.000	0.002	0.000	0.001	0.005	0.001	0.003	0.002	0.002
K	0.001	0.000	0.001	0.000	0.000	0.000	0.001	0.001	0.000	0.000	0.000	0.000	0.000
Total	3.001	3.003	3.002	3.004	2.999	3.001	3.002	2.004	2.004	2.001	2.001	2.002	2.004
X_{Usp}	2.379	2.322	2.329	2.343	2.337	2.339	2.337						
X_{Ilm}								1.557	1.538	1.589	1.551	1.548	1.547

greater than 50 % and is represented by pyroxene-hornblende gabbro. The dioritic rocks are differentiated into diorite and quartz diorite (quartz>5 %). The most remarkable feature in all the rock types is the development of secondary amphibole (e.g., actinolite) either as uralite after pyroxene (uralitization) or at the expense of primary amphibole (amphibolitization).

Pyroxene-hornblende gabbro is fine- to medium-grained and possesses hypidiomorphic granular texture. The mineral

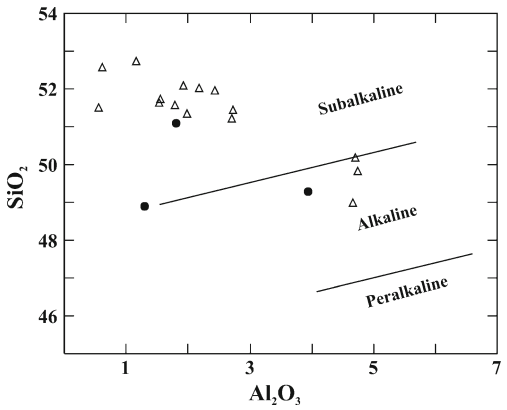

Fig. 3 SiO_2-Al_2O_3 discrimination diagram of clinopyroxenes in the studied intrusion (Le Bas 1962)

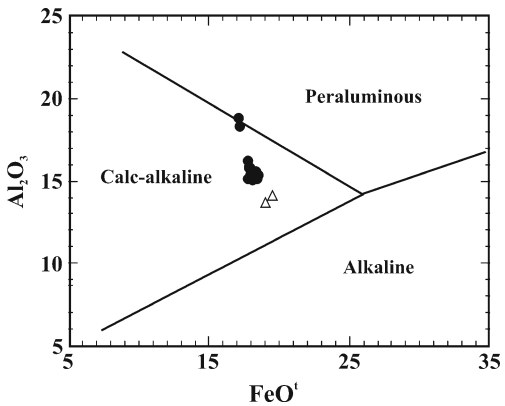

Fig. 4 FeO_t vs. Al_2O_3 biotite discriminant diagram for the analyzed biotites in rocks of the studied intrusion (Abdel-Rahman 1994)

Table 7 Chemical analyses of different rock types of the studied intrusion

Rock type	Py-Hb gabbro						Diorite		Qz-diorite									
	11	12	13	14	15	16	17A	17B	1	2	3	4A	4B	4C	4D	4E	6	7
SiO_2	48.67	47.70	45.88	45.35	47.50	47.75	55.54	55.50	58.48	59.00	58.73	58.80	57.62	59.70	58.88	59.30	58.50	58.80
TiO_2	0.52	0.50	0.22	0.35	0.35	0.45	1.28	1.18	0.95	1.00	1.00	1.00	1.12	0.90	0.93	0.98	0.96	0.88
Al_2O_3	16.22	17.20	17.96	16.07	18.60	15.03	16.57	16.12	16.82	15.61	15.78	15.70	15.56	16.66	16.06	16.25	15.60	16.62
Fe_2O_3	9.29	8.58	8.00	8.65	7.58	8.58	7.61	7.42	5.97	6.55	6.38	6.34	7.05	6.15	6.23	6.26	6.58	5.39
MnO	0.16	0.18	0.19	0.19	0.17	0.19	0.14	0.17	0.10	0.12	0.12	0.12	0.10	0.10	0.10	0.10	0.12	0.10
MgO	8.08	8.11	8.86	9.38	7.32	9.06	4.51	4.99	3.66	4.13	3.95	3.95	4.08	3.65	3.98	3.71	4.10	3.50
CaO	9.95	10.96	13.51	14.00	11.88	12.46	6.33	7.28	6.02	5.76	5.74	5.74	5.72	5.45	5.74	5.60	6.55	5.57
Na_2O	1.91	1.40	0.77	0.84	1.17	1.01	3.82	3.86	4.05	3.62	3.84	3.95	3.61	3.84	3.74	3.89	3.68	3.65
K_2O	1.59	1.63	1.08	0.98	1.74	1.64	2.13	2.03	2.26	2.54	2.40	2.46	2.71	2.75	2.60	2.80	2.54	2.52
P_2O_5	0.27	0.33	0.08	0.15	0.25	0.25	0.34	0.50	0.36	0.38	0.42	0.38	0.34	0.36	0.40	0.42	0.36	0.30
L.O.I.	3.10	2.89	2.83	3.74	3.03	3.78	1.10	1.08	1.00	0.85	0.78	1.05	1.60	0.94	0.76	0.77	0.96	1.18
Total	99.76	99.48	99.38	99.70	99.59	100.2	99.37	100.13	99.67	99.56	99.14	99.49	99.51	100.5	99.42	100.08	99.95	99.51
Mg#	61.2	63.1	66.7	66.3	63.6	65.7	51.8	54.9	52.6	53.3	52.9	53.0	51.2	51.8	53.6	51.8	53.0	54.0
Trace elements (ppm)																		
Ba	364	383	220	160	337	385	1223	1205	1027	992	1016	945	1013	1008	905	1020	954	878
Ni	82	67	66	96	83	74	112	116	83	93	89	72	87	105	104	78	86	75
Cr	273	250	226	303	188	305	137	157	123	152	129	113	117	113	121	116	125	122
Co	39	38	42	45	36	42	28	31	24	25	25	25	24	23	24	23	25	21
Nb	2	4	3	3	4	1	7	6	5	6	6	5	7	7	6	5	6	7
Rb	38	40	33	32	42	43	57	56	69	70	69	70	68	71	69	72	70	72
Sr	620	530	494	346	555	486	1050	1097	1162	967	1043	1042	1057	976	1026	1011	1009	1035
Zr	37	29	21	20	38	39	118	116	180	189	183	184	182	194	188	190	186	196
Y	7	11	6	5	7	8	15	16	18	19	18	17	16	19	18	19	17	18
V	214	226	236	240	225	220	142	140	152	171	169	164	159	152	156	158	166	141
La	5.45			7.1		8.3	26.9		26.8				31.0					
Ce	12.3			15.7		18.9	61.3		59.7				69.4					
Pr	1.60			2.17		2.59	7.33		7.25				7.99					
Nd	7.6			9.6		11.6	31.8		29.5				33.9					
Sm	2.00			2.45		3.09	5.5		5.5				5.8					
Eu	0.71			0.74		1.03	1.71		1.49				1.55					
Gd	2.29			2.45		2.97	4.03		4.39				4.27					
Tb	0.40			0.41		0.49	0.57		0.66				0.61					
Dy	2.19			2.35		2.86	2.8		3.49				3.17					
Ho	0.46			0.44		0.62	0.47		0.57				0.53					

Table 7 (continued)

Rock type	Py-Hb gabbro						Diorite		Qz-diorite							
	11	12	13	14	15	16	17A	17B	1	2	3	4A	4B	4C	4D	4E	6	7
Er	1.42			1.27		1.78	1.46		1.62				1.50					
Tm	0.21			0.18		0.26	0.21		0.24				0.23					
Yb	1.46			1.07		1.57	1.22		1.54				1.51					
Lu	0.19			0.12		0.19	0.18		0.23				0.20					
∑REE	38.28			46.05		56.25	145.48		142.98				161.66					
$(Eu/Eu^*)_n$	1.01			0.92		1.04	1.11		0.93				0.95					
$(La/Yb)_n$	2.68			4.76		3.79	15.82		12.48				14.73					
$(La/Sm)_n$	1.76			1.87		1.73	3.16		3.15				3.45					
$(Ce/Yb)_n$	2.34			4.08		3.34	13.96		10.77				12.77					

constituents (Table 1) are plagioclase (50–59 vol%), amphibole (17–37 vol%), pyroxene (4–13 vol%), biotite (3–7 vol%) and opaques (~3 vol%). Others are chlorite and epidote.

Plagioclase occurs as large tabular crystals that may reach 4 mm in length, usually with albite and albite-Carlsbad twinning. Most of these plagioclase crystals exhibit alteration to epidote and sericite. Amphibole is commonly of green color exhibiting pleochroism variable in green; i.e., yellow green, olive green to dark green and is mainly actinolite-tremolite, replacing primary clinopyroxene. Clinopyroxene occurs as subhedral crystals uncommonly display simple twinning. It is mainly decomposed to secondary amphibole around its margin. The opaque Fe-Ti oxides are represented by homogeneous magnetite as discrete euhedral crystals; rare fine grains of ilmenite are recorded.

Diorite and quartz diorite more or less have the same texture, habit and characteristics of the essential minerals. However, quartz content is higher in quartz diorite (7–10 vol%) than in diorite (3–5 vol%). Both contain few (1–4 vol%) subhedral to anhedral K-feldspar occur between plagioclase. Diorite and quartz diorite are holocrystalline, mainly equigranular hypidiomorphic of medium-grained size. The modal compositions of both rock types are plagioclase (64–71 vol%), amphibole (7–13 vol%), biotite (4–7 vol%), clinopyroxene (1–3 vol%), and opaques (2.5–4 vol%). Secondary phases are chlorite and epidote.

The plagioclase occurs as subhedral tabular crystals displaying albite and albite-Carlsbad twinning and is partly altered to sericite. Hornblende is anhedral with bluish green to light yellow pleochroism and partly replaced by actinolite and Fe-Ti oxides. Quartz occurs as interstitial grains with sutured outlines and shows undulatory extinction. Biotite co-exists with amphibole and forms discrete anhedral to subhedral crystals and crystal aggregates. Pyroxene is a minor consistent and exhibits marginal alteration to secondary amphibole (uralitization). The opaque minerals are represented by homogeneous subhedral ilmenite grains.

Mineral chemistry

Chemical composition of essential minerals was determined by electron probe microanalysis (EPMA) using CAMERA SX 100 instrument under operating conditions of 15 kV and 20 nA. Suitable synthetic and natural standards were applied for calibration. The analyses were carried out at the Institute of Mineralogy, Claustal University, Germany. The raw data were processed through Minpet Software after Richard (1995) for the calculation of the given structural formulae.

Representative microprobe analyses of essential mineral phases from the investigated rocks are given in Tables 2, 3, 4, 5, and 6.

Feldspars

Feldspars were analyzed from pyroxene-hornblende gabbro and dioritic rocks (diorite and quartz diorite). The analyzed feldspars in the pyroxene-hornblende gabbro are represented mainly by bytownite; while in the diorite are andesine. In quartz diorite, both plagioclase and alkali-feldspar are present. Plagioclase is mainly oligoclase and the alkali-feldspar is almost pure orthoclase with rare anorthoclase.

Pyroxenes

All pyroxenes of the pyroxene-hornblende gabbro and diorite are clinopyroxenes with very narrow compositional range from diopside to augite according to the classification of Morimoto (1988). The majority of the analyzed clinopyroxenes plot in the subalkaline field on the SiO_2 vs. Al_2O_3 diagram of Le Bas (1962) (Fig. 3).

Amphiboles

The amphiboles of the pyroxene-hornblende gabbro and the dioritic rocks are primary and secondary amphiboles. Primary amphiboles are high in TiO_2 and all contain >0.1 Ti p.f.u. (Girardeau and Mevel 1982), whereas secondary amphiboles have low TiO_2, contain <0.1 Ti p.f.u. According to the classification of Leake (1997) all analyzed amphiboles are calcic, primary amphiboles in the pyroxene-hornblende gabbro are magnesio-hornblende and tschermakite, while secondary amphiboles in both gabbro and diorite are actinolite and magnesio-hornblende. In the dioritic rocks, the rare primary amphiboles are magnesio-hornblende.

Biotites

Biotites were analyzed from the gabbros and dioritic rocks. They have a restricted compositional range. Biotite composition reflects the composition of the parent magma (Abdel-Rahman 1994). According to the classification of Abdel-Rahman (op. cit.), the analyzed biotites are similar to those of calc-alkaline suites having moderate enrichment of MgO with FeO*/MgO=1.8. The FeO*/MgO ratios of biotites range between 1.33 and 1.59 with an average of 1.46, which is nearly similar to that of calc-alkaline biotites. On the Al_2O_3 vs. FeO_t biotite discrimination diagram, the analyzed biotites plot also in the field of calc-alkaline suite (Fig. 4).

Fe-Ti oxides

Fe-Ti oxides were analyzed from the pyroxene-hornblende gabbro and quartz diorite. The analyzed Fe-Ti oxides include magnetite and ilmenite. Primary magnetite is characteristically abundant in gabbros, whereas it is nearly absent in dioritic rocks and only occurs as fine grains at expense of decomposed ferromagnesium silicates. Magnetite analyzed from pyroxene-hornblende gabbro has low TiO_2 contents (0.03–0.26 %). The ulvöspinel contents in the magnetite, calculated according to Stromer (1983), are below 2.4 mol%. End-member components (X_{ilm} and X_{hem}) of ilmenite are calculated according to Stromer (1983). The analyzed ilmenite is nearly pure ilmenite (0.90–0.94 % mole ilmenite) and enriched in MnO content (2.60–3.68 wt.%) relative to the magnetite.

Geochemical characteristics

Eighteen samples representing the different lithologies of gabbro/diorite intrusion at Sheikh El-Arab area (6 gabbro, 2 diorite, and 10 quartz diorite) were selected for major and trace element chemical analyses. Major oxides compositions and Ba, Co, Nb, Ni, Sr, Y, and Zr were analyzed using inductively coupled plasma-emission spectrometry (ICP-ES). The remainder of trace elements and the rare earth elements (REE) were determined using inductively coupled plasma-mass spectrometry (ICP-MS) following a lithium metaborate/tetraborate fusion and nitric acid digestion of a 0.2 g sample. All analyses were determined at ACME Analytical Laboratories Limited, Vancouver, Canada. Loss on ignition (L.O.I.) was determined by heating powdered samples for 50 min at 1000 °C. The analytical precision, as calculated from duplicate samples is better than ±1 % for the major elements and ±5 % for most trace elements.

Chemical analyses of representative rock samples are given in Table 7. The studied rocks have a wide range of composition. Pyroxene-hornblende gabbro contains 45–49 wt.% SiO_2, diorite contains about 55 wt.% SiO_2, while quartz diorite contain 58–60 wt.% SiO_2 (Fig. 5). The

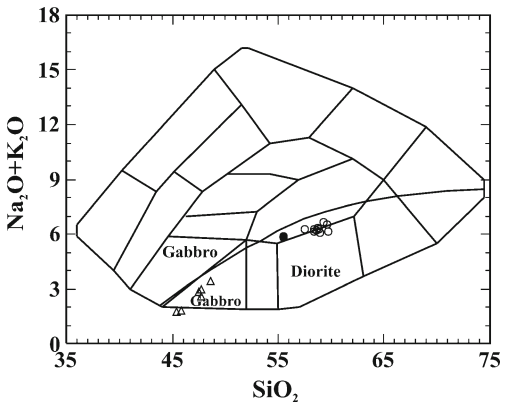

Fig. 5 TAS diagram for the studied rocks (Cox et al. 1979); adopted by Wilson (1994). The dividing *line* between alkalic and subalkalic magma series from Miyashiro (1978)

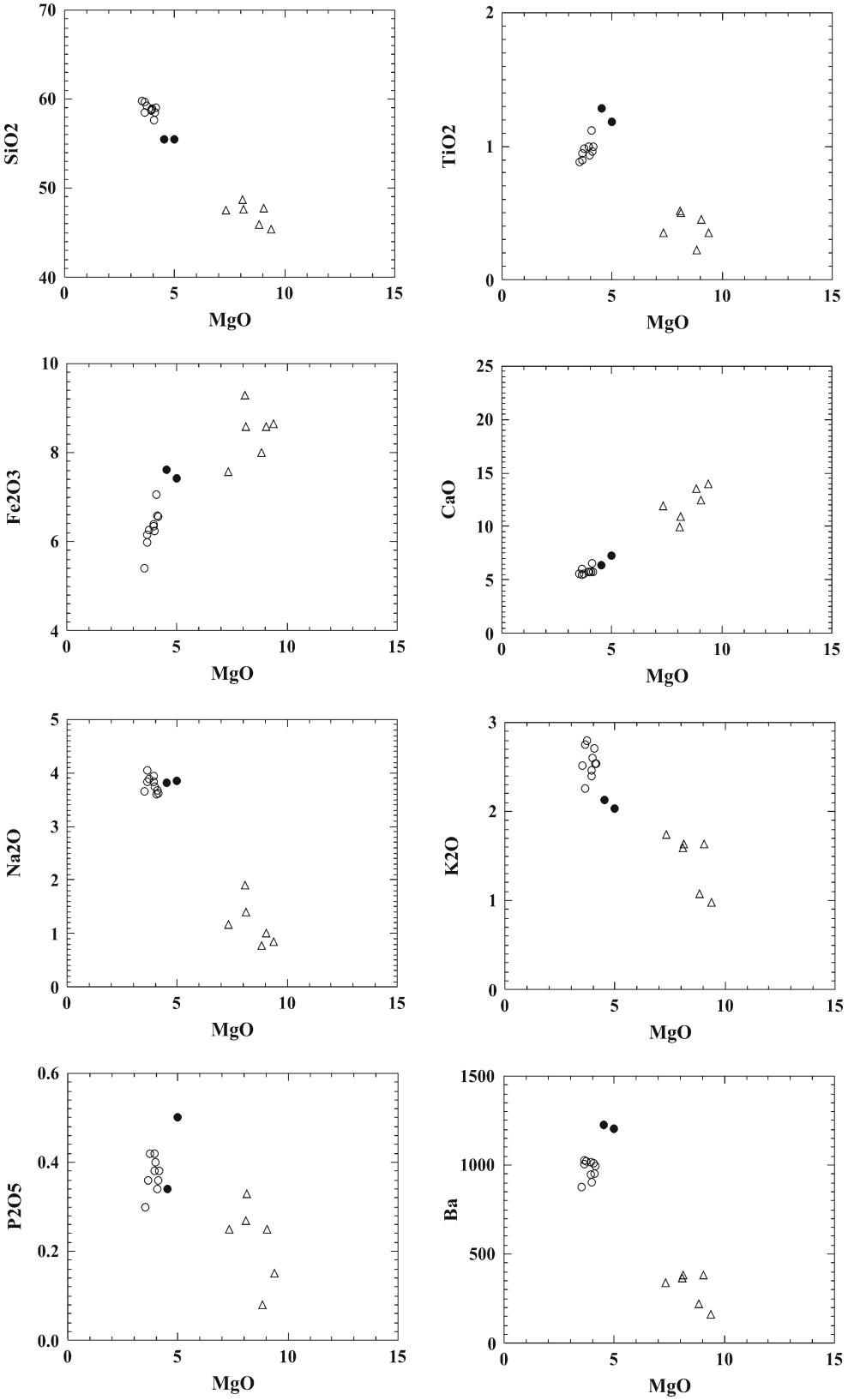

Fig. 6 MgO vs. major and selected trace elements plots

gabbros have the highest contents of Fe_2O_3, MgO, CaO, Cr, Co, and V. Variation diagrams (Fig. 6) show that compositional trends of the studied intrusion are consistent with their mineralogical compositions. Fe_2O_3, CaO, Cr,

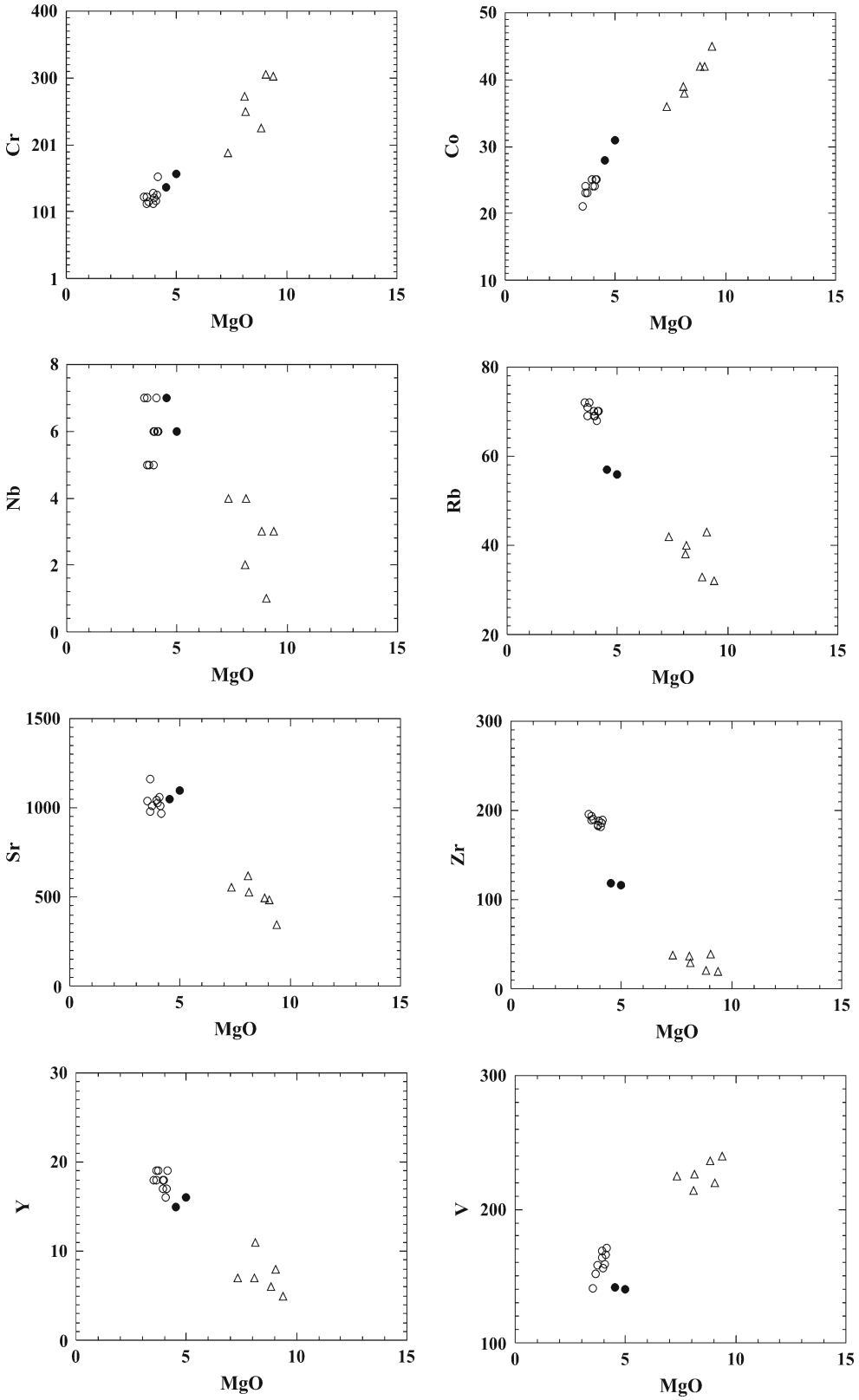

Fig. 6 (continued)

Co, and V covary with MgO while SiO_2, TiO_2, Na_2O, K_2O, P_2O_5, Ba, Rb, Sr, Nb, Zr, and Y antivary with MgO. The variation trends imply that fractionation crystallization has a prominent role in the evolution of the

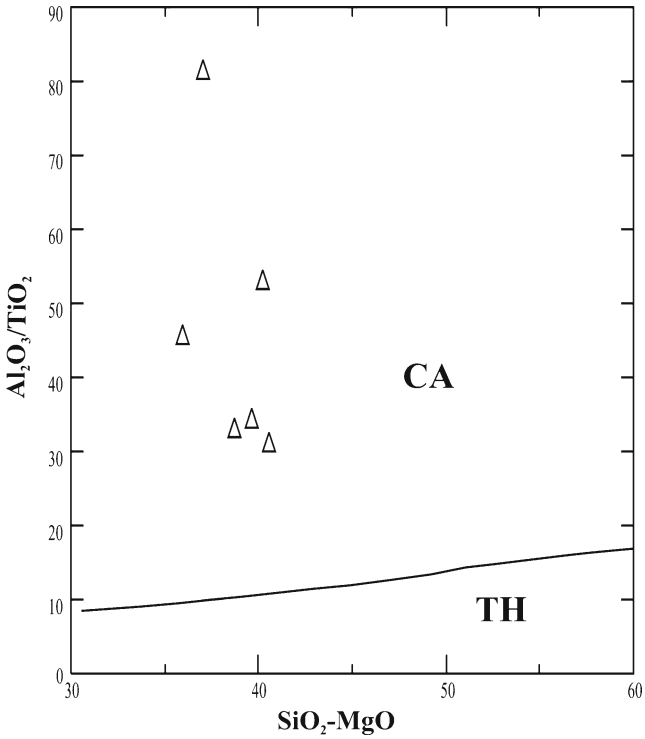

Fig. 7 (SiO_2-MgO) vs. (Al_2O_3/TiO_2) classification *diagram* for the studied gabbros (Middlemost 1997)

studied rocks. The increase of Sr and decrease of CaO with increasing differentiation index suggest that fractionation of mafic minerals (e.g., pyroxene and amphibole) greatly predominated over plagioclase (Whalen 1985). This is consistent with the positive correlation of SiO_2 with Sr (partitioned in plagioclase) which indicate that plagioclase was of minor importance as a crystallizing phase during the fractional crystallization. It is to be noted here that the more evolved member of the suite (dioritic rocks) has exceptionally higher TiO_2 contents than the gabbros. This can be attributed either to

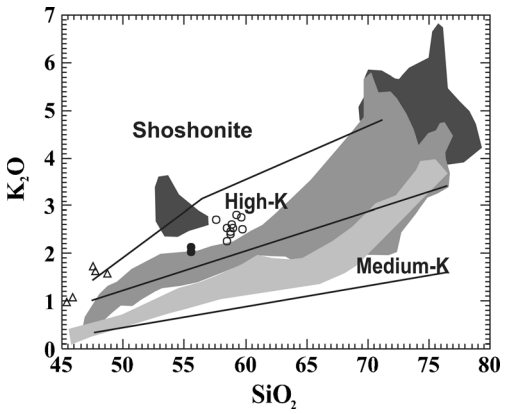

Fig. 8 SiO_2 vs. K_2O classification *diagram* with the *boundary lines* after Le Maitre (IUGS 1989) and Rickwood (1989). IAC *light gray*; CA1 *dark gray Medium-K*; CA2 *dark gray High-K*; AL *black High-K and shoshonitic series*

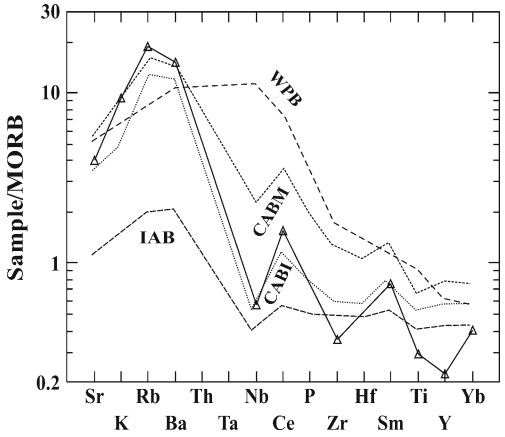

Fig. 9 NMORB-normalized spider diagram showing comparison of element distribution for the average of studied gabbros with basalts from different tectonic settings (Condie 1997)

the possibility of simultaneous assimilation of the country rocks and fractional crystallization, or to the gradual decrease of the oxygen fugacity during the evolution of the suite. The decrease of the oxygen fugacity may explain the near absence of magnetite in the more evolved member where ilmenite becomes the predominant opaque phase.

Major- and trace element discriminant diagrams have developed for the recognition of basaltic rocks from various tectonic settings. Although strictly applicable only to volcanic rocks, such methods can provide constrains for our plutonic rocks. Most of the analyzed gabbros define a transitional trend between the calc-alkaline and tholeiitic affinity on the AFM diagram (not shown), while the diorites and quartz diorites have clear calc-alkaline affinity. However, on the (SiO_2-MgO) vs. Al_2O_3/TiO_2 diagram introduced by Middlemost (1997) to separate subalkalic basic and intermediate rocks into tholeiitic and calc-alkaline lineages (Fig. 7), all the analyzed gabbros have calc-alkaline nature.

The classification diagram of SiO_2 vs. K_2O (Fig. 8) with the boundary lines after Le Maitre (IUGS 1989) and

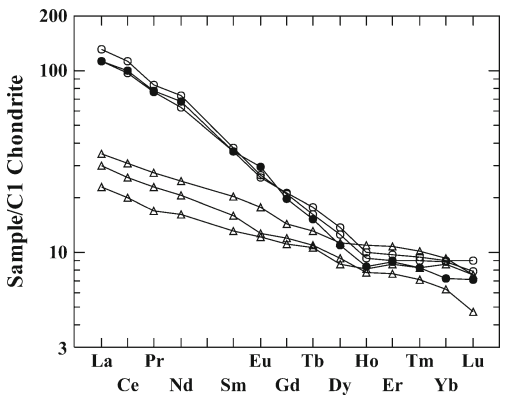

Fig. 10 Chondrite-normalized REE patterns for the studied gabbro/diorite suite

Rickwood (1989) was recently used by several authors (e.g., Abu Anbar 2009; Be'eri-Shlevin et al. 2009a, b; Eyal et al. 2010; Azer et al. 2012) to differentiate between pre-, syn- and post-collisional plutonic rocks including mafic ones in south Sinai. The gabbro, diorite and quartz diorite are mostly high-K, i.e., they are related to post-collisional intrusions of late calc-alkaline batholithic stage (CA2) (e.g., Be'eri-Shlevin et al. 2009a; b; Eyal et al. 2010).

The NMORB-normalized rocks, using the normalizing values of Pearce (1983; cited in Rollinson 1993), are shown in Fig. 9. The studied rocks show enrichment of large-ion lithophile elements (LILEs—K, Rb, Ba) over the high field strength elements (HFSEs—Nb, P, Zr, Ti, Y) with a Nb negative anomaly, which is a characteristic feature of subduction-related magmas (discussed below).

The REE concentrations of six samples (Table 7) normalized to the chondrite values of Sun and McDonough (1989) are shown in Fig. 10. The pyroxene-hornblende gabbro is notably low in total REE (38.28–56.25 ppm), and about 15–22 times chondrite with $(La/Yb)_n$=2.68–4.76 and is characterized by the absence of Eu anomalies, its Eu/Eu* ratios are mostly close to unity (0.92–1.04). The analyzed samples of diorite and quartz diorite are high in total REE (145.48 and 142.98–161.66 ppm, respectively) and about 57 and 56–63 times chondrite with remarkably high $(La/Yb)_n$ values of 15.82 and 12.48–14.73 and accompanied by absence of noticeable Eu anomalies (Eu/Eu*=1.11 and 0.93–0.95). The REE pattern of the gabbros is characterized by moderately fractionated pattern, while the dioritic rocks show strongly fractionated pattern.

Discussion

In south Sinai, the metamorphic complexes were intruded by calc-alkaline (CA) and alkaline (AL) magmas. The calc-alkaline magmatism is considered as syn- to late orogenic (El-Gaby et al. 1990; Essawy et al. 1997; Azer 2007). In view of recent geochronological studies, Be'eri-Shlevin et al. (2009a, b, 2011) subdivided the CA rocks into an older suite (CA1) including variably deformed syn- to late-collisional deformed plutons and associated volcanic rocks (650–625 Ma) and a younger, post-collisional suite (CA2) ranges in age from 625 to 590 Ma and is represented by slightly deformed or undeformed plutons of granodiorite and monzogranite accompanied by minor mafic-ultramafic and dioritic intrusions. The AL magmatism (610–580 Ma) includes alkaline to peralkaline felsic and rare intermediate and mafic plutons together with bimodal dyke swarms. The AL magmatism is associated with the tectonic transition to extensional regime. Eyal et al. (2010) indicated that CA and AL magmatism occurred at 635–590 Ma and 608–580 Ma, respectively.

The gabbro/diorite pluton at Sheikh El-Arab area, intruded by the Rahaba granodiorite (610 Ma; Be'eri Be'eri-Shlevin et al. 2009a), is most probably related to post-collisional calc-alkaline suite, even without direct geochronological data yet. The intrusion enclosed xenoliths of variably sheared and foliated metasediments and volcanics of the lower unit of Rutig Formation (ca. 630–615 Ma; Be'eri-Shlevin et al. 2011). It is undeformed and unmetamorphosed, but subjected to late-magmatic and subsolidus alteration. This is consistent with the view that the onset of calc-alkaline post-collisional magmatism occurred at ~620 Ma in the western Feiran-Solaf area and at ~610 Ma at the eastern Kid area (Eyal et al. 2014). The mafic-intermediate intrusion at Gebel Sheikh El-Arab area contains volcanic and clastic xenoliths of Rutig Formation and intruded the calc-alkaline syntectonic granodiorite, therefore it is regarded as post-collisional (post-tectonic setting) intrusion. It was emplaced, most probably, at a late stage of calc-alkaline magmatism. Generally, the post-collisional plutons are undeformed and post-date accretion and the beginning of the inferred orogenic collapse (Blasband et al. 2000), and thus they are regarded as batholithic, post-collisional intrusions. Importantly, El-Gaby (2007) pointed out that after the accretion event, the amount of tholeiitic basalts decrease drastically among the associated calc-alkaline volcanics. Likewise the amount of tholeiitic gabbros decreases relative to the associated cal-alkaline plutonic rocks. This may explain the transitional trend between calc-alkaline and tholeiitic character for the studied gabbros on some variation diagrams (e.g., AFM and Y-Zr diagrams).

Late-magmatic alteration

Many primary minerals in the studied suite display evidence of complex late-magmatic and subsolidus reactions. These transformations are particularly noticed in the gabbros where for example the pyroxene of the pyroxene-hornblende gabbros is frequently decomposed to secondary amphibole around their margin (uralitization). In addition, secondary amphibole (actinolitic hornblende) is developed at the expense of primary hornblende (amphibolitization) in all rock types of the suite. Subsolidus saussuritization of plagioclase is manifested by their replacement by clinozoisite and zoisite having low pistacite mole fraction (Ps=0.01–0.04) (Johnston and Wyllie 1988). Chloritization of ferromagnesian minerals is distributed in the studied rocks.

The petrographically recorded late-magmatic alteration signature of the studied rocks must be evaluated in order to consider that the given mineralogical and chemical data are

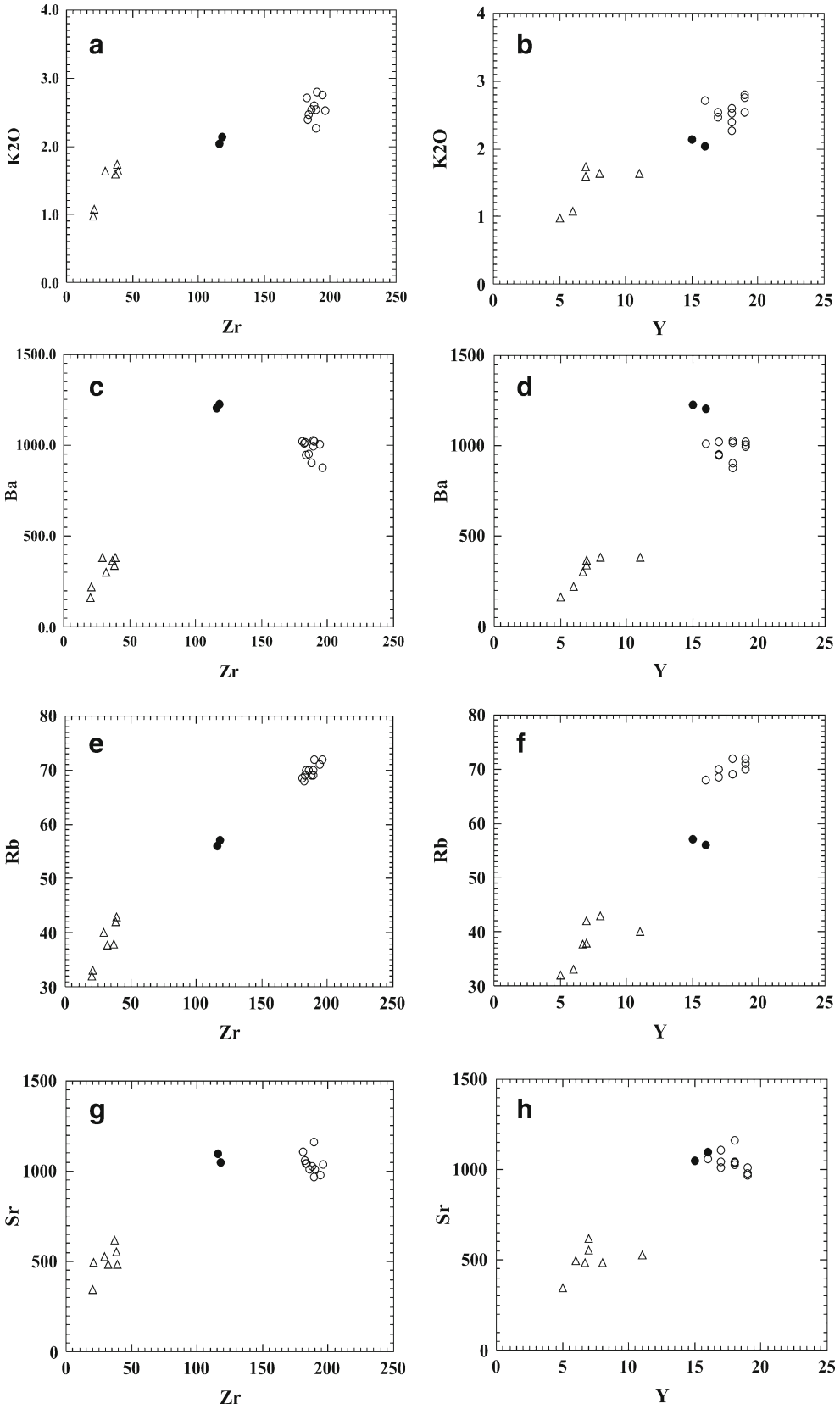

Fig. 11 Interelemental relations between LILE (K, Rb, Ba and Sr) and HFSE (Zr and Y) of the studied suite

still meaningful. The elemental variation diagrams of the mobile LILE and the relatively immobile HFSE can furnish to some extent the degree of alteration processes. Generally, from the variation diagrams of Y or Zr against K, Ba, Rb, and

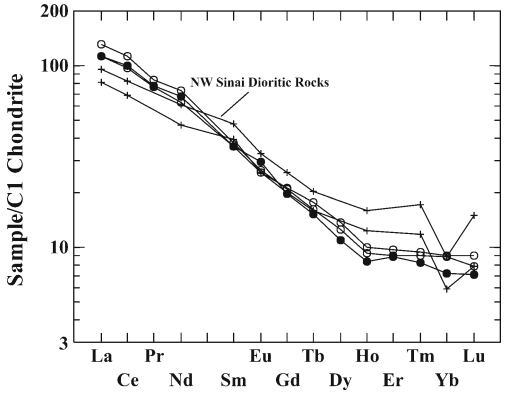

Fig. 12 Chondrite-normalized REE plots of the studied diorites and NW Sinai diorites (El-Sayed 2003)

Sr (Fig. 11, a–h), it is evident that evolution fractionation trend can be traced from the pyroxene-hornblende gabbro to the diorite then to the quartz diorite. Only Ba deviates from the given trends with respect to both Zr and Y. However, the overall trends suggest that the alteration did not significantly modify their original chemical compositions. Therefore, the chemical composition of the suite can approximately reflect their source characteristics.

Tectonic setting

Field relations of gabbro/diorite suite at Sheikh El-Arab area reveal that the rocks are undeformed and unmetamorphosed. This indicates post-collisional characteristics for the intrusion where it intruded syntectonic granodiorite. The chemical characteristics that were not severely affected by alteration refer to the high-K calc-alkaline nature. This is consistent with the view that the post-collisional magmatic stage through the ANS commenced with the emplacement of high-K calc-alkaline intrusions (Bentor 1985; Stoeser and Camp 1985; Stern and Abdelsalam 1998; Moghazi et al. 1998; Moghazi 2002; Jarrar et al. 2003; Eyal et al. 2010). Thus, the studied intrusion

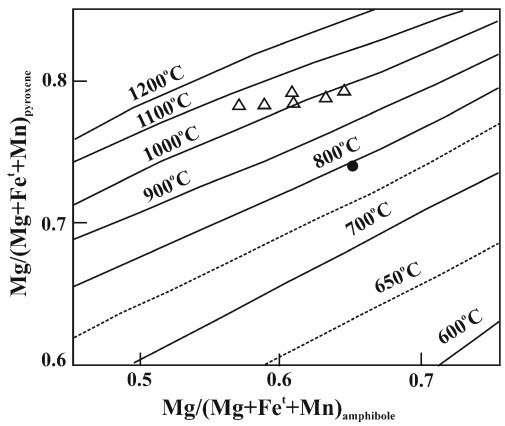

Fig. 13 Geothermometry using coexisting primary amphibole-pyroxene pairs (Perchuk 1970; in Urlych et al. 1976)

belongs to the post-collisional batholithic calc-alkaline late stage (CA2) lasted in south Sinai from ~619 to 592 Ma (Eyal et al. 2010). The post-collisional tectonic setting is also evidenced from the chemical composition of mafic minerals (clinopyroxene and biotite) where they are of subalkaline character similar to those of post-orogenic gabbroic rocks in south Sinai (Abu Anbar 2009; Azer and El-Gharbawy 2011; Azer et al. 2012). The dioritic rocks of the studied post-collisional intrusion have comparable contents of REE and their patterns are rather identical with post-collisional dioritic rocks of NW Sinai (Fig. 12) (El-Sayed 2003) with similar average values of $(Eu/Eu^*)_n$ (0.99 and 0.93) and $(La/Yb)_n$ (14.3 and 12.3).

Primary magma and crystallization conditions

The petrographic and geochemical studies revealed that the intermediate-mafic rocks at Gebel Sheikh El-Arab area are comagmatic and underwent fractional crystallization. The gabbros have higher Mg# values (av. 64.43) than the diorites (av. 53.35) and quartz diorites (av. 52.72). High Wo contents (41.73–51.69) of the clinopyroxenes indicate that these minerals of the analyzed gabbros are near-liquidus crystallization products of water-bearing basaltic magmas (Sisson and Grove 1993). This is accompanied by the presence of anorthite-rich plagioclase ($An_{80–83}$) suggesting a liquid composition that was high in Al and H_2O and low in Na (Sisson and Grove op. cit.). The crystallization of hornblende was occurred by increasing H_2O in magma after crystallization of clinopyroxene and Ca-rich plagioclase. Thus, the gabbro/diorite rocks were the products of low pressure fractional crystallization process from gabbroic parent magma.

The gabbros at Gebel Sheikh El-Arab area have low Nb (1–4 ppm), Zr (20–39 ppm) and Y (5–11 ppm), geochemically similar to subduction-related setting (Pearce 1983), since subduction is not considered plausible in the post-collisional tectonic setting in south Sinai, the subduction signature for the studied rocks may be due to partial melting of lithospheric mantle enriched during a previous subduction event in the ANS (Friz-Töpfer 1991; Stein et al. 1997; Be'eri-Shlevin et al. 2009a; Eyal et al. 2010; Azer et al. 2012).

The variation diagrams of the analyzed rocks show increase of Fe_2O_3, CaO, Cr, Co, and V with the increase of MgO, while TiO_2, Na_2O, K_2O, Ba, Rb, Sr, Nb, Y, and Zr decrease. These trends indicate that fractional crystallization of mafic magma is the main process controlling the magma evolution; simultaneous assimilation and/or gradual decrease in oxygen fugacity accounted to the observed variation.

The field relations, mineralogy and geochemistry of the studied gabbro/diorite intrusion indicate its similarity to the calc-alkaline post-collisional gabbro/diorite intrusions and belonging to the second calc-alkaline substage (late substage) of Eyal et al. (2010). These post-collisional calc-alkaline mafic

intrusions have slightly positive ЄNd(T) values ranging from +2.4 to +4.5 indicating that the source was probably depleted lithospheric mantle with minor crustal component (Eyal et al. 2010).

The coexisting clinopyroxene and primary amphibole in pyroxene-hornblende gabbro and diorite yields approximate crystallization temperatures around 1000–1050 and 800 °C, respectively, using the diagram given by Perchuk (1970; in Urlych et al. 1976) (Fig. 13).

In sum, the gabbro/diorite suite at Sheikh El-Arab area is related to the later calc-alkaline substage of post-collisional tectonic setting. It is not related to the mafic-ultramafic suite as previously thought (cf. Soliman 1996; Abdel-Karim 2013).

Conclusion

The gabbro/diorite intrusion at Sheikh El-Arab area represents the only mafic exposure in the basement rocks (mainly granitoids and their volcanic equivalents) of central Sinai. The intrusion is undeformed and unmetamorphosed, but experienced uralitization and amphibolitization. Field relations indicate that the intrusion postdates the lower unit of the volcano-sedimentary succession of the Rutig Formation and predates the surrounding rocks related to the late phase of calc-alkaline magmatism or to the alkaline Katharina outer ring dike. Pyroxene-hornblende gabbro, diorite, and quartz diorite are the main rock types of the studied intrusion.

Mineralogically, bytownite and andesine represent the plagioclase of the analyzed gabbros and diorites, respectively. Oligoclase and orthoclase are the main feldspars in the quartz diorite. Diopside-augite represents the clinopyroxenes of the studied rocks and their compositions indicate the subalkaline nature of their parent magma. Both primary and secondary amphiboles are present. Biotites have restricted compositional range and are similar to that of calc-alkaline biotites. The analyzed magnetite has low TiO_2 content, and the ilmenite is nearly pure ilmenite and enriched in MnO content.

Geochemically, the studied gabbro/diorite suite is high-K and is related to post-collisional tectonic setting. The subduction-related signature for the studied rocks is most probably due to the partial melting of a lithospheric mantle enriched during a previous subduction event in the ANS. The whole series of the studied rocks were the products of fractional crystallization process from gabbroic parent magma, accompanied by assimilation and/or gradual decrease in oxygen fugacity during their evolution.

From initial mafic magma, the crystallization of hornblende was caused by H_2O increase in magma after crystallization of near-liquidus clinopyroxene having high Ca content ($Wo_{42–52}$) and Ca-rich plagioclase ($An_{80–83}$).

Several geochemical lines of evidence suggest that the main process that controlled the evolution of the gabbro magma was mainly fractional crystallization. The systematic compositional variations are revealed by the variation diagrams of the suite. Total REE abundances increase from the least evolved gabbro (38–56 ppm) to the most evolved dioritic rocks (143–162 ppm) can also be explained in terms of fractional crystallization. The REE data for both the gabbros and diorites indicate that this fractionation could have been extensive for the diorites as their REE patterns are highly fractionated relative to the gabbros. The higher Mg# in gabbros (61–67) relative to dioritic rocks (51–55) argues in favor of fractional crystallization as the dominant process in magma evolution. The rocks of the suite are characterized by low Ni contents (66–116 ppm), low Mg# (51–67) variable and wide range of Cr contents (113–305 ppm) consistent with their derivation from upper mantle with subsequent modification by fractional crystallization. The depleted HREE contents in the suite suggest the presence of residual garnet in the mantle source.

Petrographically, the investigated rocks exhibit hypidiomorphic texture with no apparent layering and lack cumulate texture. Geochemically, they lack positive Eu anomalies and have relatively high incompatible element contents. These rocks may thus be considered to represent near-liquidus compositions rather than cumulates, derived from melting of depleted upper mantle source.

The studied intrusion contains volcanic and clastic xenoliths of the older Rutig Formation indicating its high level of emplacement. Crystallization temperatures are between 1000 and 1050 °C for the gabbros and 800 °C for the diorites. The intrusion is related to the later calc-alkaline substage of post-collisional tectonic setting. It is not related to the mafic-ultramafic suite as previously thought.

Acknowledgments The facilities offered by the Institute of Mineralogy, Claustal University, Germany for EPMA, are greatly appreciated. We are grateful to the remarks from the anonymous reviewer who improved the manuscript.

References

Abdel-Karim AM (2013) Petrology, geochemistry and petrogenetic aspects of younger gabbros from south Sinai: a transition from arc to active continental margin. Chem Erde 73:89–104

Abdel-Rahman AM (1994) Nature of biotites from alkaline, calc-alkaline and peraluminous magmas. J Petrol 35:525–541

Abdel-Rahman AM (1995) Tectonic-magmatic stages of shield evolution: the Pan-African belt in northeastern Egypt. Technophysics 242: 223–240

Abu Anbar MM (2009) Petrogenesis of the Nesryin gabbroic intrusion in SW Sinai, Egypt: new contributions from mineralogy, geochemistry, Nd and Sr isotopes. Mineral Petrol 95:87–103

Azer MK (2007) Tectonic significance of late Precambrian calc-alkaline and alkaline magmatism in Saint Katherina area, South Sinai, Egypt. Geol Acta 5:255–272

Azer MK, El-Gharbawy RI (2011) Contribution to the Neoproterozoic layered mafic-ultramafic intrusion of Gabal Imleih, south Sinai, Egypt: implication of post-collisional magmatism in the north Arabian-Nubian Shield. J Afr Earth Sci 60:253–272

Azer MK, Abu El-Ela FF, Ren M (2012) The petrogenesis of late Neoproterozoic mafic dyke-like intrusion in south Sinai, Egypt. J Asia Earth Sci 54–55:91–109

Basta EZ, Takla MA (1974) Distribution of opaque minerals and the origin of the gabbroic rocks of Egypt. Bull Fac Sci Cairo Univ 47: 347–364

Be'eri-Shlevin Y, Katzir Y, Whitehouse M (2009a) Post-collisional tectono-magmatic evolution in the northern Arabian-Nubian Shield: time constraints from ion-probe U-Pb dating of zircon. J Geol Soc Lond 166:71–85

Be'eri-Shlevin Y, Katzir Y, Valley JW (2009b) Crustal evolution and recycling in a juvenile continent: oxygen isotope ratio of zircon in the northern Arabian Nubian Shield. Lithos 107:169–184

Be'eri-Shlevin Y, Samuel MD, Azer MK, Rämö OT, Whitehouse MJ, Moussa HE (2011) The Ediacaran Ferani and Rutig volcano-sedimentary successions of the northernmost Arabian-Nubian Shield (ANS): new insights from zircon U-Pb geochronology, geochemistry and O-Nd isotope ratios. Precambrian Res 188:21–44

Bentor YK (1985) The crust evolution of the Arabo-Nubian Massif with special reference to the Sinai Peninsula. Precambrian Res 28:1–74

Beyth M, Stern RJ, Altherr R, Kröner A (1994) The late Precambrian Timna igneous complex, southern Israel: evidence for comagmatic-type sanukioid monzodiorite and alkali granite magma. Lithos 31: 103–124

Blasband B, White SH, Brooijmans P, Visser W, de Boorder H (2000) Late Proterozoic extensional collapse in the Arabian-Nubian Shield. J Geol Soc Lond 157:615–628

Condie KC (1997) Plate tectonics and crustal evolution, 4th edn. Butterworth-Heinemann, Oxford, p 282

Cox KG, Bell JD, Pankhurst RJ (1979) The interpretation of igneous rocks. Allen and Unwin, London, p 450

El-Gaby S (2007) Integrated classification and evolution of the Neoproterozoic Pan-African belt in Egypt. Int Conf Geol Afr 1: 143–154

El-Gaby S, List FK, Tehrani R (1988) Geology, evolution and metallogenesis of the Pan-African belt in Egypt. In: El-Gaby S, Greiling R (eds) The Pan-African belt of NE Africa and adjacent areas tectonic evolution and economic aspects. Vieweg, Braunschweig, Wiesbaden, pp 17–68

El-Gaby S, List FK, Tehrani R (1990) The basement complex of the Eastern Desert and Sinai. In: Said R (ed) The geology of Egypt. Balkema, Rotterdam, pp 175–184

El-Sayed MM (2003) Neoproterozoic magmatism in NW Sinai, Egypt: magma source and evolution of collision-related intracrustal anatectic leucogranite. Int J Earth Sci (Geol Rundsch) 92:145–164

Essawy MA, El-Metwally AA, Katta LA, Darwish NK (1997) Younger granites and pegmatites from Taba area, southeastern Sinai, Egypt. Egypt J Geol 41:495–518

Eyal M, Bartov Y, Shimron AE, Bentor YK (1980) Sinai geological map, aeromagmatic map. Geol Surv Israel 1:500,000, 1 sheet, scale

Eyal M, Litvinovsky B, Jahn BM, Zanvilevich A, Katzir Y (2010) Origin and evolution of post-collisional magmatism: coeval Neoproterozoic calc-alkaline and alkaline suites of the Sinai Peninsula. Chem Geol 269:153–179

Eyal M, Bentor YK, Goor A, Bruner I, Eyal Y, Calvo R, Hall JK, Rosensaft M (2013) Geological map of Katherina ring complex, Sinai, Egypt. Geol Surv Israel 1:50,000, 1 sheet, scale

Eyal M, Be'eri-Shlevin Y, Eyal Y, Whitehouse MJ, Litvinovsky B (2014) Three successive Proterozoic island arcs in the northern Arabian-Nubian Shield: evidence from SIMS U-Pb dating of zircon. Gondwana Res 25:338–351

Farahat ES, Zaki R, Hauzenberger C, Sami M (2011) The Neoproterozoic calcalkaline peraluminous granitoids of the Deleihimmi pluton, Central Eastern Desert, Egypt: implications for transition from late- to post-collisional tectonomagmatic evolution in the northern Arabian-Nubian Shield. Geol J 46:544–560

Friz-Töpfer A (1991) Geochemical characterization of Pan-African dyke swarms in southern Sinai: from continental margin to intraplate magmatism. Precambrian Res 49:281–300

Girardeau J, Mevel C (1982) Amphibolitized sheared gabbros from ophiolites as indicators of the evolution of the oceanic crust: bay of islands, Newfoundland. Earth Planet Sci Lett 61:151–165

IUGS (1989) In: Le Maitre RW (ed) A classification of igneous rocks and glossary of terms: recommendations of the international union of geological sciences sub-commission on the systematics of igneous rocks. Blackwell, Oxford, p 193

Jarrar GH, Stern RJ, Saffarini G, Al-Zubi H (2003) Late and post-orogenic Neoproterozoic intrusions of Jordan: implications for crustal growth in the northernmost segment of the East African Orogen. Precambrian Res 123:295–319

Johnson PR, Woldehaimanot B (2003) Development of the Arabian-Nubian shield: perspectives on accretion and deformation in the northern East African Orogen and the assembly of Gondwana. In: Yoshida M, Windley BF, Dasgupta S (eds) Proterozoic East Gondwana: Supercontinent Assembly and Breakup: Spec Pub. Geol Soc London 206, pp. 289–326

Johnston AD, Wyllie PJ (1988) Interaction of granitic and basic magmas: experimental observations on contamination processes at 10 kbar with H_2O. Contrib Mineral Petrol 98:352–362

Kröner A (1985) Ophiolites and the evolution of tectonic boundaries in late Proterozoic Arabian-Nubian Shield of Northeast Africa and Arabia. Precambrian Res 27:277–300

Le Bas MJ (1962) The role of aluminum in igneous clinopyroxenes with relation to their parentage. Am J Sci 260:267–288

Leake BE (1997) Nomenclature of amphiboles: report of the subcommittee on amphiboles of the international mineralogical association commission on new minerals and mineral names. Mineral Mag 61:295–321

Meert JG (2003) A synopsis of events related to the assembly of eastern Gondwana. Teconophy 362:1–40

Middlemost EAK (1997) Magmas, rocks and planetary development. Longman, 299 p

Miyashiro A (1978) Nature of alkalic rock series. Contrib Mineral Petrol 66:91–104

Moghazi AM (2002) Petrology and geochemistry of Pan-African granitoids, Kab Amiri area, Egypt—implications for tectonomagmatic stages of the Nubian Shield evolution. Mineral Petrol 75:41–67

Moghazi AM, Andersen T, Oweiss GA, El-Bouseily AM (1998) Geochemical and Sr-Nd-Pb isotopic data bearing on the origin of Pan-African granitoids in the Kid area, southeast Sinai, Egypt. J Geol Soc Lond 155:697–710

Moreno JA, Montero P, Abu Anbar M, Molina JF, Scarrow JH, Talavera C, Cambeses A, Bea F (2012) SHRIMP U-Pb zircon dating of the Katerina ring complex: insights into the temporal sequence of Ediacaran calc-alkaline to peralkaline magmatism in southern Sinai, Egypt. Gondwana Res 12:887–900

Morimoto N (1988) Nomenclature of pyroxenes. Mineral Petrol 39:55–76

Moussa EMM, Stern RJ, Manton WI, Ali KA (2008) SHRIMP zircon dating and Sm/Nd isotopic investigations of Neoproterozoic granitoids, Eastern Desert Egypt. Precambrian Res 160:341–356

Pearce JA (1983) Role of the subcontinental lithosphere in magma genesis at active continental margins. In: Hawkesworth CJ, Norry MJ (eds) Continental basalts and mantle xenoliths. Shiva, Nantwich, pp 230–249

Richard LR (1995) Mineralogical and petrological data processing system. minpet software (c) 1988–1995, Version 2.02

Rickwood PC (1989) Boundary lines within petrologic diagrams which use oxides of major and minor elements. Lithos 22:247–263

Rollinson H (1993) Using geochemical data: evaluation, presentation, interpretation. Longman Scientific & Technical—Wiley, New York, p 352

Samuel MD, Be'eri-Shlevin Y, Azer MK, Whitehouse MJ, Moussa HE (2011) Provenance of conglomerate clasts from the volcano-sedimentary sequence at Wadi Rutig in southern Sinai, Egypt as revealed by SIMS U-Pb dating of zircon. Gondwana Res 20:450–464

Sisson TW, Grove TL (1993) Experimental investigations of the role of H_2O in calc-alkaline differentiation and subduction zone magmatism. Contrib Mineral Petrol 113:143–166

Soliman F (1996) Geology of Wadi Tarfa-Wadi Isla region, southern Sinai, Egypt. M.E.R.C. Ain Shams Univ: Earth Sci Ser 10:214–228

Stein M, Navon O, Kessel R (1997) Chromatographic metasomatism of the Arabian-Nubian lithosphere. Earth Planet Sci Lett 152:75–91

Stern RJ (1994) Arc assembly and continental collision in the Neoproterozoic East African orogen. Implications for the consolidation of Gondwanaland. Ann Rev Earth Planet Sci 22:319–351

Stern RJ, Abdelsalam MG (1998) Formation of continental crust in the Arabian-Nubian Shield: evidence from granitic rocks of the Nakasib suture, NE Sudan. Geol Rdsch 87:150–260

Stern RJ, Hedge CE (1985) Geochronologic and isotopic constraints on late Precambrian crustal evolution in the Eastern Desert of Egypt. Am J Sci 285:97–127

Stoeser DB, Camp VE (1985) Pan-African microplate accretion of Arabian shield. Geol Soc Am Bull 96:817–826

Stoeser DB, Frost CD (2006) Nd, Pb, Sr, and O isotopic characterization of Saudi Arabian Shield terranes. Chem Geol 226:163–188

Stromer JC Jr (1983) The effects of recalculation on estimates of temperature and oxygen fugacity from analyses of multicomponent iron-titanium oxides. Am Miner 68:586–594

Sun S, McDonough WF (1989) Chemical and isotopic systematics of the oceanic basalts: implications for mantle composition and processes. Magmatism in the Ocean Basins. In: Saunders AD, Norry MJ (eds) Geol Soc London, Spec Publ 42, pp. 313–345.

Takla MA (2002) Economic potentialities of the Shield and Phanerozoic rocks of Egypt. 6th Inter Conf Geol Arab World, Cairo Univ XXXII–XXXIII

Takla MA, Basta EZ, Fawzi E (1981) Characterization of the older and younger gabbros of Egypt. Delta J Sci 5:279–314

Takla MA, Basta FF, Madbouly MI, Hussein AA (2001) The mafic-ultramafic intrusions of Sinai, Egypt. Ann Geol Surv Egypt 24:1–40

Urlych J, Cimbálníkova A, Fiala J, Kaspar P, Lang M, Minarík L, Palivcová M, Pivec E (1976) Petrology of the Petrovice melagabbro. Rozpr Cs Akad Ved R mat Prír Ved Academia, Praha, p 57

Whalen JB (1985) Geochemistry of an island-arc plutonic suite: the Vasilau-Yau Yau intrusive complex, New Britain, P.N.G. J Petrol 26:603–632

Wilson M (1994) Igneous petrogenesis. Chapman and Hall, London, p 466